Project Title:

Innovative compact HYbrid electrical/thermal storage systems for low energy BUILDings

Project Acronym:

HYBUILD

Grant Agreement N°: 768824

Collaborative Project

Deliverable Report

Deliverable number:

D3.1

Deliverable title:

Modular flow sheet simulation of the hybrid (sub-)system

Related task:	3.1
Lead beneficiary:	AIT
Authors and institutions in alphabetical order:	AIT - Johann Emhofer and Tilman Barz ITAE - Valeria Palomba, Andrea Frazzica and Francesco Sergi NTUA - Stratis Varvagiannis and Sotirios Karellas UDL - Eduard Oro, Gabriel Zsembinszki and Luisa F. Cabeza
Due date:	30th of September, 2018

DISSEMINATION LEVEL		
PU	Public, fully open, e.g. web	X
CO	Confidential, restricted under conditions set out in Model Grant Agreement	
CI	Classified, information as referred to in Commission Decision 2001/844/EC.	

European Commission

This is part of the project that has received funding from the European Union's Horizon 2020 research and innovation programme *under grant agreement No 768824.*
The content of this document reflects only the author's view and the Commission is not responsible for any use that may be made of the information it contains.

Table of contents

Publishable executive summary

HYBUILD is an EU Horizon 2020-funded project, led by COMSA Corporación, which will develop two innovative compact hybrid electrical/thermal storage systems for stand-alone and district connected buildings.

Deliverable 3.1 provides a comprehensive description of the simulation models for dynamic flowsheet simulations of the HYBUILD hybrid sub-systems. The presented models are our tools to develop and design the individual components on the one hand and the detailed schemes of the sub-systems on the other hand. In this report, we show how connections of individual developed components to sub-systems with basic control strategies are realized and discuss them with the aid of typical examples. By means of lab-scale experiments in WP2 and WP3, the presented models will be validated in the upcoming months. Figure 1 shows a Mediterranean - and Figure 2 shows a Continental-type hybrid sub-system realized in the Dymola/Modelica environment.

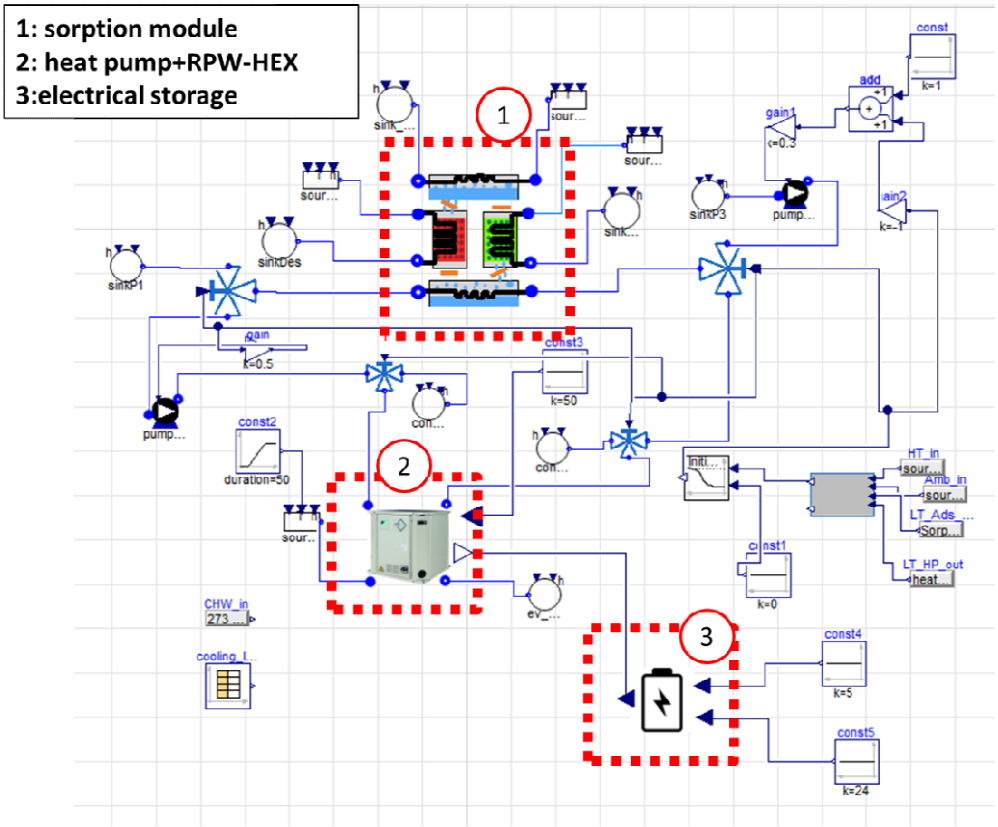

Figure 1: Scheme of a Mediterranean-type hybrid sub-system in Dymola/Modelica

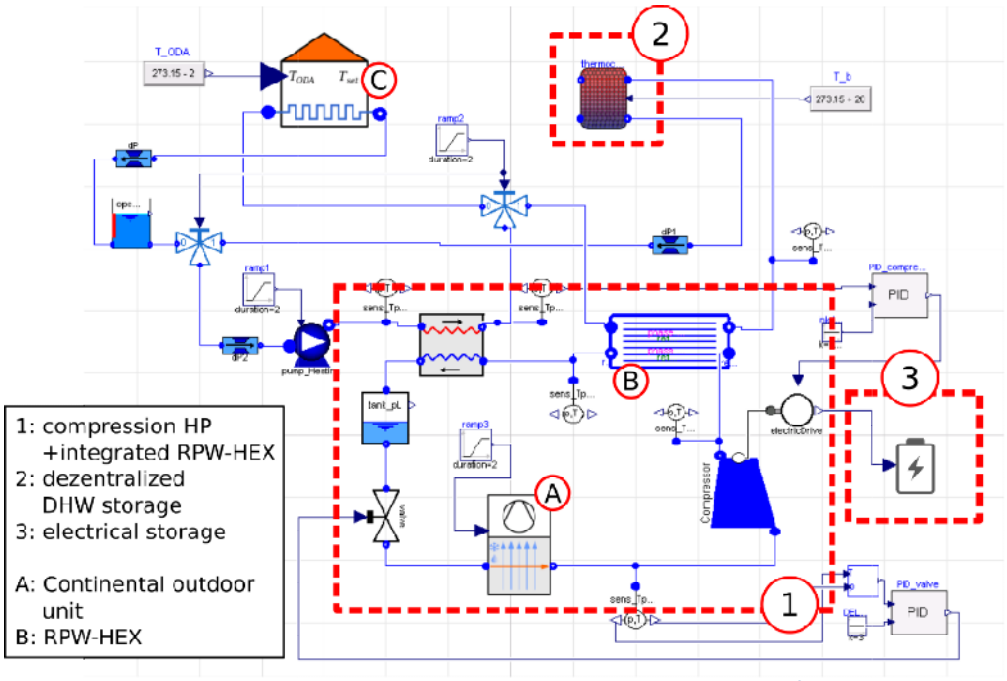

Figure 2: Scheme of a Continental type hybrid sub-system in Dymola/Modelica

Methodology

All participating partners agreed on using Modelica as a modelling language for the dynamic flow sheet simulations. When possible, models from the open source Modelica Standard Library (MSL) and the open source Thermocycle-library were used to describe the sub-systems and their components. All developed components within Task 3.1 are compatible to the mentioned existing libraries to guarantee quick adaptions and extension of the concept at a later point of time. The models needed to be developed for the HYBUILD systems are:

- Adsorption module for the Mediterranean concept: It comprises two adsorbent reactors, connected to a condenser and an evaporator. The model simulates both heat and mass transfer phenomena inside each component. A preliminary validation of the adsorber model was performed against literature data. The whole module is represented by (1) in Figure 1 and is controlled by a basic control unit.
- Compression heat pump model for the Mediterranean concept using a moving boundary method: A vapour compression cycle model of the Daikin heat pump, including an evaporator, a condenser, a compressor and an expansion valve. The heat exchanger dynamic models were developed based on the Moving Boundaries method in order to increase the simulation efficiency of the integrated Mediterranean system, the compressor model is steady state based on the isentropic and volumetric efficiency concepts, while the expansion valve was implemented using a PID controller. In addition, a three-way valve model was implemented in order to revert hydraulically the machine's operation from chilling to heating mode. The model was calibrated against Daikin's performance data. The unit is represented by (2) in Figure 1
- Continental outdoor unit considering the ice aggregation during winter: A finned tube air source HEX is used as an evaporator to extract renewable heat from air during winter. Currently, no Modelica models are available that consider frost aggregation and defrosting in an air source evaporator and therefore, this component was developed in Task 3.1. In order to reduce the simulation time, a quasi-static approach was used to model the ice aggregation. The frost growth and densification perpendicular to the

refrigerant flow direction was solved analytically whereas the refrigerant flow was discretized in 1D. The developed evaporator integrated in the heat pump cycle is denoted as component (A) in Figure 2.

- Refrigerant-PCM (Phase Change Material)-Water-Heat Exchanger (RPW-HEX) module for the Mediterranean and the Continental concept: The RPW-HEX consists of a 3-fluid (refrigerant, PCM, and water) heat exchanger, which has different functionalities depending on the working conditions. The internal design consists of a parallel arrangement of rectangular passages for water and refrigerant with rectangular layers of PCM in between. Fluid passages and PCM layers are arranged sequentially. In order to study the thermal behaviour of the RPW-HEX, one 2D numerical model was developed for each of the three possible working modes. Because of symmetry of the RPW-HEX design, only the relevant section of the entire component was considered in the model, which considers solely one refrigerant + water + PCM layer. The RPW-HEX integrated in the heat pump cycle is denoted as component (B) in Figure 2.
- Electrical storage model for the Mediterranean and Continental concepts: It is an analytical model based on an equivalent electric circuit, able to simulate the electrochemical behaviour of the battery in terms of voltage and current. Furthermore, it was improved to consider the effect of high current rate discharging on the overall capacity of the battery. Preliminary validation of the model was performed using experimental results available at ITAE. The component is represented by (3) in Figure 1 and Figure 2.
- Auxiliary models needed for the simulations:
  - Simple building model: This model represents a connection to WP4 and the demo-site data. Besides the usage of controlled thermal sources and sinks, we present two different methods to include the demo specific data. One is suited for application on a sub-seconds time scale (e.g. for basic control) and the other one is suited for calculations on a yearly timescale (e.g. for techno-economic analysis) or for generating performance maps. The first one, can be directly included in the dynamic models (e.g. (C) in Figure 2). It uses heat transfer correlations and neglect solar radiation for the sake of simplicity. The second method shows a way to reduce simulation data over one year with a data binning method to calculate a yearly efficiency with a reduced set of operating conditions and the developed models.
  - Charge controller: This model regulates the energy flow of the electrical storage according to some of its main operating parameters (e.g. voltage, current, state of charge). Based on the input values and some standard reference parameters, the charge controller allows three working mode of the battery: charging, discharging or self-consumption.

Most of the developed models solve the equations for mass-, energy- and momentum conservation using a 1D – Finite Volume Method (FVM) approach. As mentioned before, solely the model for the Continental outdoor unit uses furthermore quasi-static equations to consider the frost growth in a second dimension whereas the RPW-HEX model uses a discretized 2D-grid to consider the behaviour of the PCM in the direction perpendicular to the refrigerant flow. The Mediterranean concept for the compression heat pump system follows a moving boundary approach for the condenser and the evaporator on the refrigerant side to increase simulation speed, whereas a discrete approach was chosen for the Continental system. The commercially available software Dymola was used for compilation of the Modelica code and the results were prepared with different software platforms like Dymola, Matlab, Python, etc.

Results and Conclusion:

We successfully managed to set up robust simulation tools for the assessment of both HYBUILD concepts. It is demonstrated, that all the core components and modules work in integrated systems that are representative for the HYBUILD concepts. During the next months, the developed simulation tool will streamline the planning and execution of upcoming lab-scale experiments, model validations, refinement of design and operational decisions and techno-economic analysis considering different KPIs on the sub-system level.

Acronyms and Abbreviations

AIT	Austrian Institute of Technology
BEMS	Building Energy Management System
COP	Coefficient Of Performance
DC	Direct Current
DHW	Domestic Hot Water
EC	European Commission
EEV	Electronic Expansion Valve
EU	European Union
EURAC	Eurac Research
FVM	Finite Volume Method
HEX	Heat EXchanger
HTF	Heat Transfer Fluid
ITAE	(aka CNR-ITAE) The Advanced Energy Technology Institute “Nicola Giordano”
MSL	Modelica Standard Library
NTUA	National Technical University of Athens
NBK	Nobatek, Institut National pour la Transition Énergétique et Environnementale du bâtiment
OCV	Open Circuit Voltage
PCM	Phase Change Material
PID	Proportional-Integral-Derivative
RPW-HEX	Refrigerant-PCM-Water HEX (latent storage integrated in the refrigerant cycle of a compression heat pump)
SoC	State of Charge
TEXV	Thermostatic Expansion Valve
UDL	Universidad de Lleida / University of Lleida
WP	Work Package

1 Introduction

1.1 Aims and objectives

The aim of deliverable D3.1 is to provide a comprehensive description of the simulation models needed for dynamic flowsheet simulations of the hybrid sub-systems. The presented models are our tools in WP3 to develop and design the individual components and the detailed schemes of the sub-systems. A typical component in this context is the latent storage integrated in the refrigerant cycle of the compression heat pump system (RPW-HEX) or the electric battery. In the case of the Continental concept, the thermal sub-system comprises the compression heat pump cycle working already with the integrated RPW-HEX considering basic control strategies. Finally, the hybrid sub-system integrates the battery to the thermal-sub system. This report describes all the modelled components that were developed in T3.1 and are needed to simulate the entire hybrid sub-system dynamically on a sub-seconds time scale. We show how connections of individual components to thermal and hybrid sub-systems could work with basic control strategies and discuss them with first results. Based on these models, the components of the hybrid sub-systems can be designed and first performance tests can be simulated. Because, no experiments with the components developed in HYBUILD were carried out when this report is presented (M12), the developed models represent first tools which needs to be validated with the experiments of Task 3.2 in the upcoming months.

1.2 Relations to other activities in the project

Deliverable D3.1 presents the tools to carry out the simulation tasks in WP3 (Hybrid storage sub-systems) which are involved in the development on the Core Module level and on the hybrid sub-system level (see Figure 1-1). Nearly all of the work for the present deliverable was carried out in Task 3.1 (Model based design and control).

The results of Task 3.1 will be used to design the RPW-HEX and to size the electric storage and the sorption storage for the lab scale tests on the Core Module level. Note, that this is much easier, if the entire system can already be simulated on the hybrid sub-system level. For the first design decisions also simplified building models are used to size the components. Therefore, preliminary data from the demo buildings provided by the demo partners and by WP4 are used in WP3. Based on the models developed in Task 3.1, performance maps will be created for WP4 to be used in the building simulations.

1.3 Report structure

This report describes all the models of components that were developed in order to simulate the entire hybrid sub-systems dynamically on a sub-seconds time scale.

- In **Section 2** we present all developed models:
  - Adsorption module for the Mediterranean concept
  - Compression heat pump model for the Mediterranean concept using a moving boundary method
  - Continental outdoor unit considering the ice aggregation during winter
  - RPW-HEX module for Mediterranean and Continental concept
  - Electrical storage model for Mediterranean and Continental concept
  - Auxiliary models needed for the simulations.
- In **Section 3**, we show how a connection of the individual components to a hybrid sub-system works and implement basic control strategies. We discuss the behaviour of the

systems based on first results of typical examples. We address specific challenges and include first performance considerations in the discussions.

- In **Section 4,** we discuss first experiences with the dynamic modelling of the hybrid sub-system and we provide an outlook on the future work in Task 3.1.

1.4 Contributions of partners

As work package leader of WP3, AIT is the editor of this report. Besides AIT, ITAE, NTUA and UDL have worked on the model development and hence, they have written different sub-sections of section 2 and 3 in this report. The reader can recognize who is mainly responsible for each contribution by the institution name following the title of a sub-section in parentheses. Furthermore, the partners from the demo sites (NBK, ALM, AGL) provided first data from the demo-sites collected and summarized by NBK and EURAC (WP4).

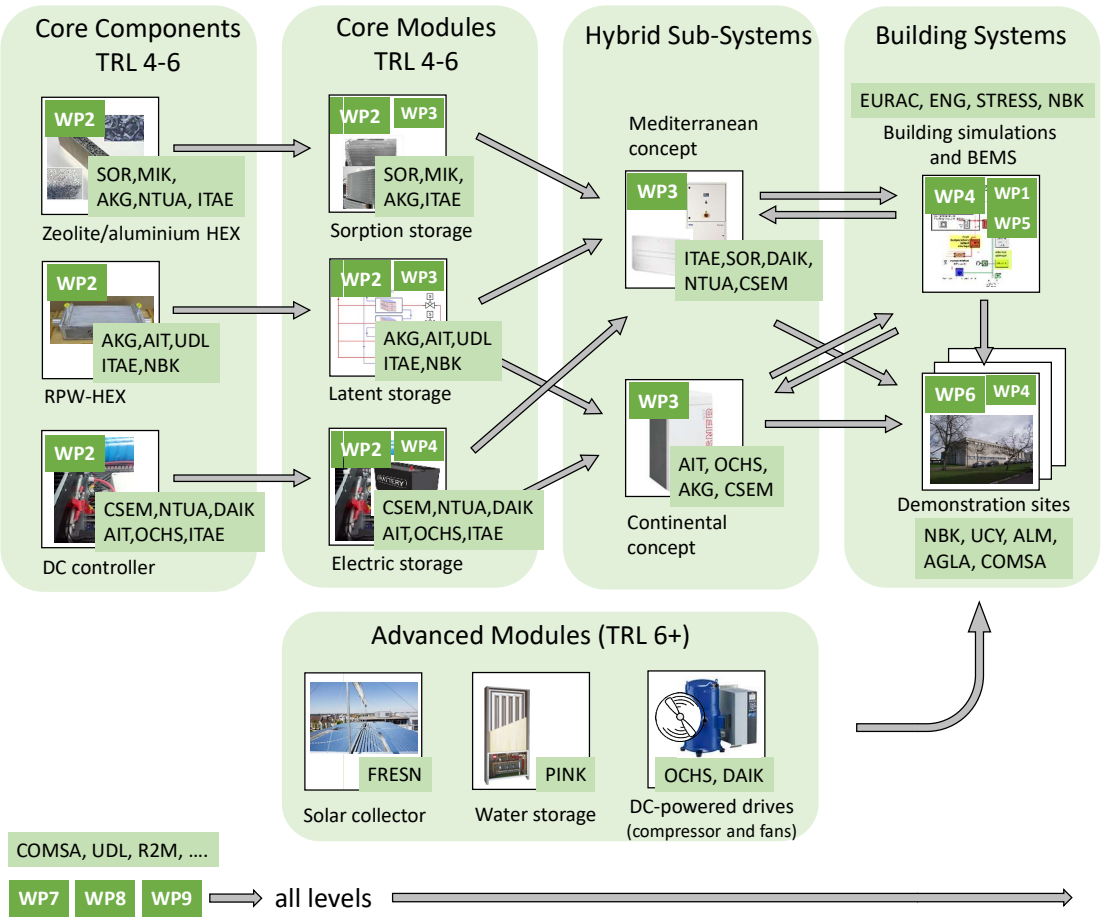

Figure 1-1: Overview of HYBUILD core components, modules, sub-systems, building systems and work packages (also shown in D4.1)

2 Individual component development and extensions of existing models

2.1 Adsorption module for Mediterranean concept (ITAE)

2.1.1 Introduction

Different modelling approaches have been proposed in earlier research for dynamic simulation of adsorption components. For instance, a commercial library containing components of thermally driven chillers is available [1] and was used to optimise the design of an adsorber using genetic algorithms [2]. However, the coupling of such type of systems with other HVAC components (i.e. vapour compression chillers, storages) has not been evaluated. It was then decided to develop a new model that:

- makes use of open source libraries and components;
- allows easy connection to other components, in particular the vapour compression chiller;
- gives the possibility to obtain useful results for the integration of the sub-system into the whole system (T4.1).

2.1.2 Methodology

The model of the adsorption module was developed in Dymola environment, using self-developed components as well as components from Thermocycle [3] and CoolProp libraries [4].

The model structure is presented in Figure 2-1. It consists of four main components and an auxiliary valve that is used to continuously refill the refrigerant into the evaporator. The main components of the model are the adsorbers, the condenser and the evaporator, each of them consisting of two sub-components: an equilibrium model and a heat exchange model. The equilibrium model is the water/water vapour equilibrium for the condenser and the evaporator and the adsorption equilibrium model, defining the uptake as a function of pressure and temperature, in the adsorber. The approach followed is similar to that proposed for adsorption chillers by [2], [5], which proved to be reliable and suitable to describe, after a proper calibration, the operation of the systems considered.

The following assumptions were made:

- all components are lumped models with uniform properties;
- the heat transfer fluid inside the heat exchangers is incompressible;
- pressure drops inside the heat exchangers are constant;
- gravity is neglected;
- the thermal masses of vacuum vessels are neglected;
- there are no heat losses to the environment;
- there is no direct heat exchanger due to conduction between the components;
- there are no inert gases inside the closed volume.

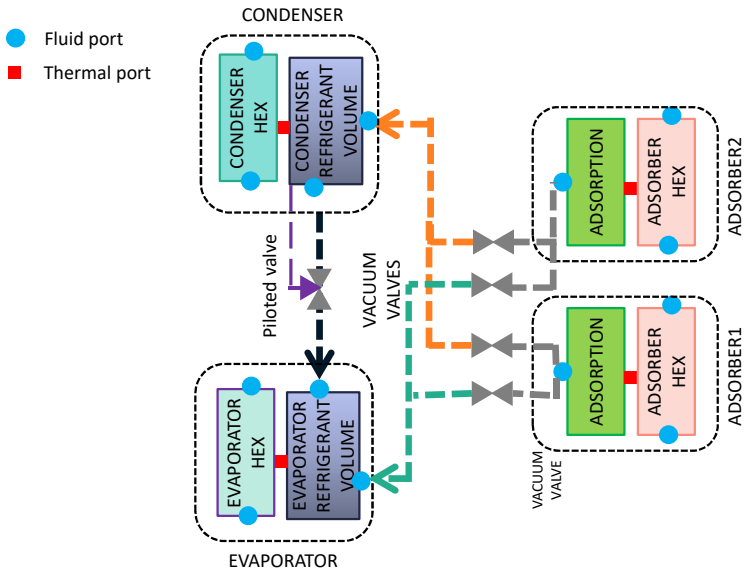

Figure 2-1: Layout of the model of the adsorption module.

2.1.3 Heat exchange model

The model for the heat exchange on the HTF side is taken from Thermocycle library.

It includes equations for mass, energy and momentum balance:

$$\dot{m}_{HTF_{in}} + \dot{m}_{HTF_{out}} = 0 \qquad \text{Eq. 2-1}$$

$$p_{HT\ _{in}} - p_{HTF_{out}} = \Delta p$$

$$\frac{dU}{dt} = \dot{H}_{HTF_{in}} - \dot{H}_{HTF_{out}} + \dot{Q}$$

with:

$$\dot{H}_{HTF} = \dot{m}_{HTF} h_{HTF} \qquad \text{Eq. 2-2}$$

$$\dot{Q} = \alpha S (T_{fluid} - T_{metal})$$

The enthalpy and the properties of the fluid are calculated from the CoolProp library, while the heat transfer coefficient α is considered constant and was estimated according to previous tests of a FAHRENHEIT unit at ITAE/CNR.

2.1.4 Adsorption equilibrium

The model for adsorption results from the mass and energy conservation inside the adsorber. Energy conservation is expressed as:

$$\left(m_{sorb} c_{p_{sorb}} + w \cdot m_{sorb} c_{p_{ref}}\right) \frac{dT_{sorb}}{dt} \qquad \text{Eq. 2-3}$$

$$= \dot{Q}_{ads} + \dot{m}_{ref} h_{ads} - m_{sorb} c_{p_{sorb}} T_{sorb} \frac{dw}{dt}$$

The terms on the left-hand side represent the sensible heat stored in the adsorbent, whereas the terms on the right-hand side represent the heat transferred through conduction and the mass exchange. For simplicity's sake, the heat of adsorption h_{ads} was considered constant.

The equilibrium conditions for temperature T_{sorb}, pressure p_{ads} and uptake w (the amount of refrigerant adsorbed onto the material) can be described by means of different equations according to the adsorbent chosen. For zeolite and zeotype materials, such as the SAPO-34 that FAHRENHEIT will synthesize on the heat exchangers with aluminium foam, one common approach is to use Dubinin-Ashtakov (DA) correlation [6]:

$$w = w_0 \exp\left[-\left(\frac{A}{E}\right)^n\right] \quad \text{Eq. 2-4}$$

where w_{max} [g/g] and n [-] are empirical constants and A [kJ/mol] is the adsorption potential:

$$A = -RT_{sorb} \log \frac{p_{ads}}{p_{sat}} \quad \text{Eq. 2-5}$$

The flow rate of refrigerant adsorbed is a function of the uptake variation in time:

$$\dot{m}_{ref} = m_{sorb} \frac{dw}{dt} \quad \text{Eq. 2-6}$$

Adsorption kinetics is described by means of a Linear Driving Force (LDF) approach [7]:

$$\frac{dw}{dt} = \beta(w_{eq} - w) \quad \text{Eq. 2-7}$$

where the constant β [t^{-1}] is calculated as [6]:

$$\beta = \frac{15}{r^2_{sorb}} D \quad \text{Eq. 2-8}$$

Where D [m^2 s^{-1}] is a diffusion coefficient. Saturation properties of the refrigerant are calculated using CoolProp library.

A schematic representation of the adsorber model, including the fluid and thermal ports, the input and output parameters and variables is shown in Figure 2-2.

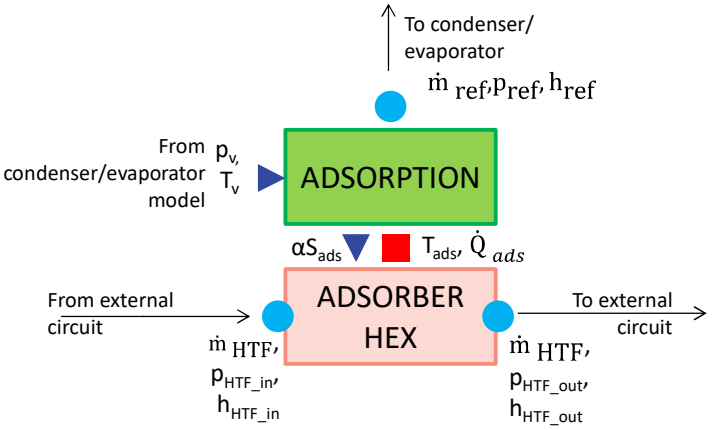

Figure 2-2: Schematic representation of the model of the adsorber.

2.1.5 Water/water vapour equilibrium model

The condenser and the evaporator of the adsorption module consist of a vacuum vessel with a heat exchanger partially immersed into the liquid refrigerant. Hence, the dominant phase change mechanism is pool boiling [8]. As for the case of the adsorber, the heat exchanger with the HTF was modelled using the equations reported in 2.1.3. Differently, the refrigerant volume takes into account the phase change and the compressibility of the medium. Mass and energy balance can be written as:

$$\frac{dm}{dt} = \dot{m}_v + \dot{m}_l \qquad \text{Eq. 2-9}$$

$$\frac{dU}{dt} = \dot{H}_v + \dot{H}_l + \dot{Q} \qquad \text{Eq. 2-10}$$

In the case of the condenser, the incoming fluid is vapour at the temperature of the adsorber and the outlet fluid is liquid having saturation enthalpy. Conversely, in the case of the evaporator, the incoming fluid is liquid at the temperature of the condenser and the outlet fluid is vapour having saturation enthalpy.

The term $\dot{Q}$ [W] represents the heat flow between the saturated refrigerant the surface of the heat exchanger:

$$\dot{Q} = \alpha S(T_{refrigerant} - T_{metal}) \qquad \text{Eq. 2-11}$$

All the properties of the refrigerant in the liquid and vapour state are calculated from CoolProp library.

A detailed schematic representation of the model of the condenser and evaporator, including the fluid and thermal ports, the input and output parameters and variables is shown in Figure 2-3.

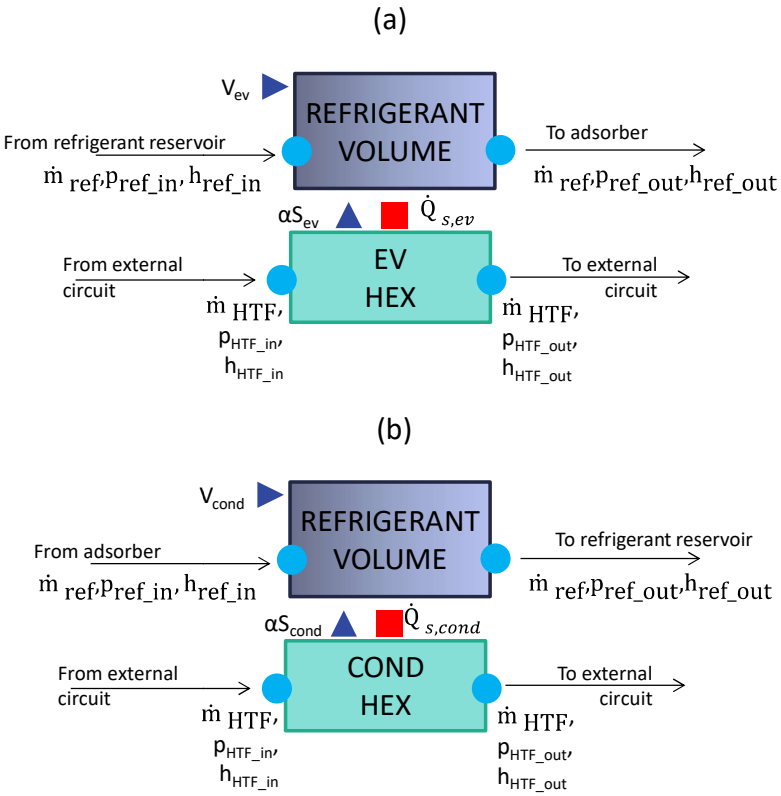

Figure 2-3: Schematic representation of the models of the evaporator (a) and the condenser (b) of the adsorption module.

2.1.6 Auxiliary components

In addition to the models of the main components in the module, some auxiliary components were used. Particularly, for the vacuum valves, a model of a valve with linear correlation from pressure drops taken from Thermocycle library was used:

$$\dot{m}_{ref} = f_v \Delta p \qquad \text{Eq. 2-12}$$

Moreover, in order to continuously transfer the refrigerant from the evaporator to the condenser, a controlled valve was inserted, using the basic code from a similar component in the SorpLib library [1]. The mass flow rate in the valve depends linearly on the difference between the level of liquid refrigerant in the condenser l and the desired level l_{set}:

$$\dot{m}_{ref} = f_p (l - l_{set}) \qquad \text{Eq. 2-13}$$

2.1.7 The adsorption module

A picture of Dymola diagram of the adsorption module is shown in Figure 2-4. As it is possible to notice, apart from the main components described in the previous sections, the sources and sinks for the hydraulic circuits, the controls for the valves and temperature sensors are included.

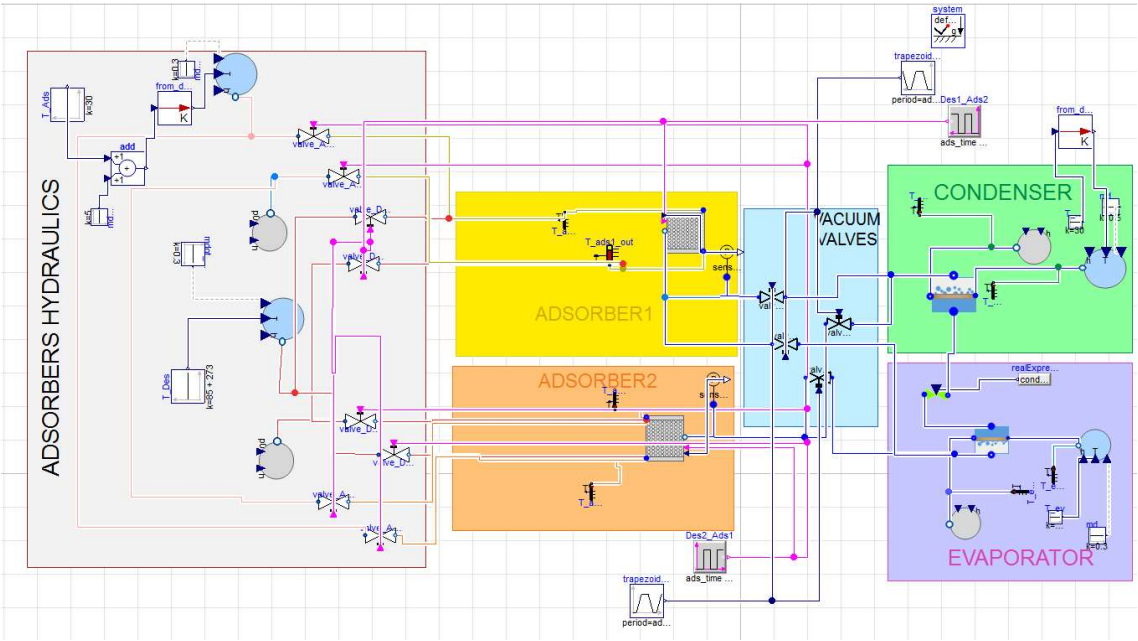

Figure 2-4: Dymola diagram of the adsorption module.

2.1.8 Interface to the hybrid subsystem model

The realized model of the adsorption module should be integrated with the other components in the sub-system, e.g. the heat pump model (including, in turn, the RPW-HEX model). Hence, it was necessary to allow easy coupling with such components. The interface of the module with the rest of the other components is represented by the fluid ports in the hydraulic circuits of the adsorbers, the condenser and the evaporator that were defined as external connectors.

A picture of the interface, taken from the "Icon" diagram of Dymola is shown in Figure 2-5. The connections for the other components are represented from the blue circles, which are the fluid ports of Thermocycle library.

Indeed, in the implementation of the model, the necessity to connect it to the other components was achieved by taking care of different aspects:

- the utilization of the same library for the fluid as in the model of the heat pump and the RPW-HEX;
- the utilization of the same connectors (i.e. the thermal and fluid ports) as in the other components;
- the utilization of the same heat transfer correlations for the heat exchangers model, taken from Thermocycle library.

This allows the consistency between the different components of the sub-system realized and simplifies setting up the simulation of the hybrid subsystem.

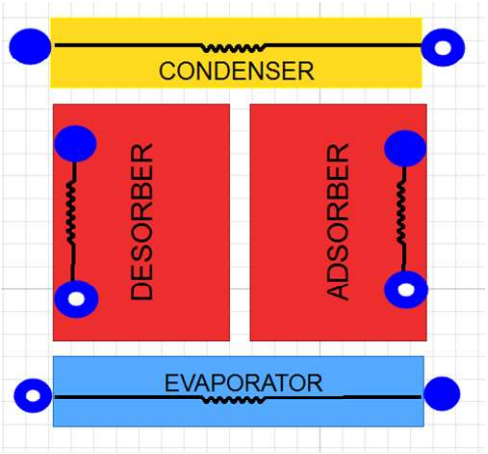

Figure 2-5: Interface of the adsorption module to the hybrid subsystem.

2.1.9 Model validation

A first validation of the model was performed on the adsorber. In particular, the results for zeolite AQSOA FAM Z02® on dynamic measurement done at ITAE and described in [9] were used. It was decided to use these data for the model validation, since the same approach will be followed in WP2 to test small-scale adsorbers employing the synthesized zeolite over the aluminum foams. The results of the experiments report the weight loss/gain of the adsorber during a typical adsorption step.

The results of the validation are reported in Figure 2-6 for a case of AQSOA FAM Z02® with grain size of 0.700-0.810 mm. It is possible to notice that the model can accurately describe the dynamic behavior of the system, the deviation with experiments being around 7.5%, which is within uncertainty of measurement, which is represented by the light red band in the picture.

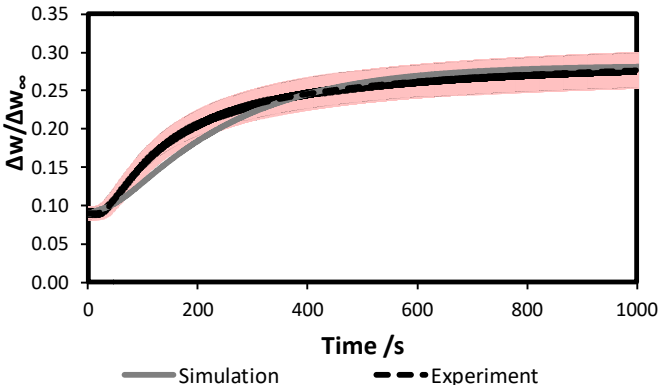

Figure 2-6: Validation of the model of the adsorber.

2.1.10 Typical example

Figure 2-7 shows the temperatures in the main components of the adsorption module for heat source temperature of 90°C, condenser inlet temperature of 30°C and evaporator inlet temperature of 15°C. The cycle time chosen is 600 s, which was selected based on kinetic considerations, in order to complete at least 80% of the theoretical uptake adsorption/release

during each phase. As it is possible to notice, the temperatures are stable and in line with the expected operation.

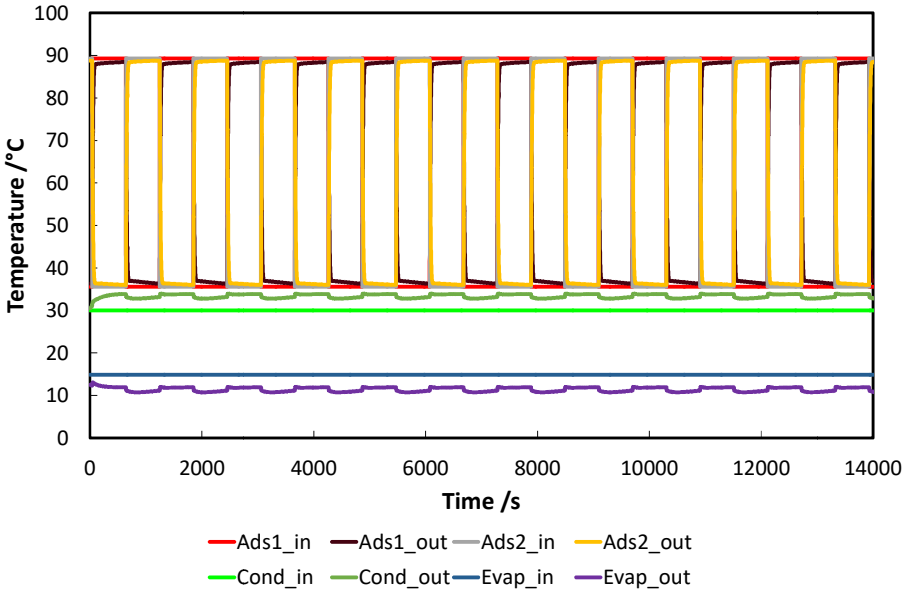

Figure 2-7: Temperatures in the adsorbers, condenser and evaporator of the adsorption module for a reference cycle.

2.1.11 List of parameters used in the model

Table 2-1 shows the list of parameters used in the model together with the reference sources they are taken from.

Table 2-1: Parameters used in the model of the thermal adsorption unit.

Parameter	Value	Source
α_{ads}	120 W m^{-2} K^{-1}	[2], [10]
$c_{p_{sorb}}$	10^3 J kg^{-1}	[11]
D	$3.3 \cdot 10^{-10}$ m^2 s^{-1}	Experimental data fitting parameter
h_{ads}	$2.6 \cdot 10^6$ J kg^{-1}	[6]
b	$5.1 \cdot 10^{-6}$ kg J^{-1}	[11]
w_0	0.4031 kg kg^{-1}	[11]
f_v	10^{-5} m s	Assumption
f_p	0.1 kg s^{-1}	Assumption

2.2 Compression heat pump module for Mediterranean concept (NTUA)

2.2.1 Introduction

Various dynamic models of compression heat pumps, developed in different simulation environments, are quite common in literature. The main objective of the model developed for the Mediterranean concept heat pump is to obtain a simple and fast model using an open source library, ensuring its interconnection with the rest of the components' models of the Mediterranean system. Since at least the evaporator of the heat pump will be substituted by the Refrigerant-PCM-Water heat exchanger (RPW-HEX, modeled by UdL), the main idea was to use simple models for the heat exchangers, capable to calibrate the heat pump exploiting Daikin's performance tables and to simulate its operation in standalone mode (e.g. during the startup of the integrated system), without increasing the model's complexity.

2.2.2 Methodology

The model of the heat pump is based on the acausal modeling technique and it was implemented in Modelica, using the Dymola interface and the open source library Thermocycle [3]. The fluid properties have been calculated with CoolProp using the ExternalMedia library. The majority of the components are self-developed or modified versions of standard ThermoCycle components. More information regarding the modeling methodology of each component is given in the following subsections:

2.2.2.1 Heat Exchanger Models

The modeling approach followed for the heat exchangers is the Moving Boundaries technique. Moving boundaries models are generally faster compared to finite volume implementations, without loss in model's accuracy [12].

The moving boundary implementation used follows the equations described by Willatzen [13], which are valid under the following assumptions:

- The velocity of the fluid is uniform on the cross sectional area
- The enthalpy of the fluid is linear in each region of the tube (sub-cooled, two-phase, super-heated)
- Pressure is considered constant in both streams
- The mean void fraction for the working fluid is constant

As an enhancement to the original equations proposed by Willatzen and similarly to the standard moving boundary implementation in ThermoCycle, the heat transfer between the primary and the secondary fluid is calculated by means of ε-NTU method, instead of calculating it using the temperature difference between the corresponding cells.

Next, the equations describing the Condenser model will be listed since the Evaporator model is identical to the condenser model, apart from having two zones instead of three (since the refrigerant enters the evaporator in two phase state), which reduces the differential equations and the states of the model from 8 to 5.

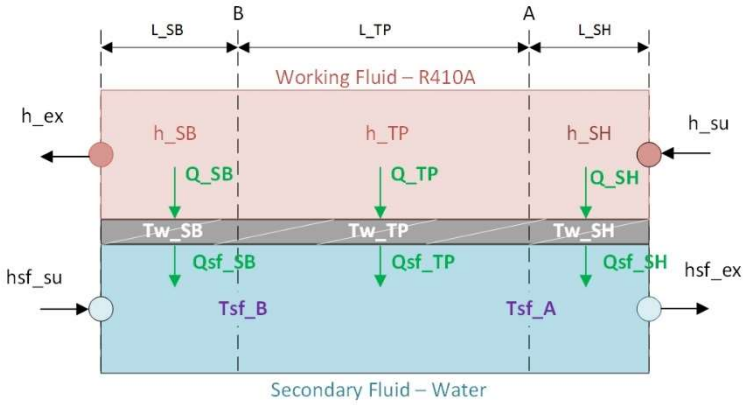

Figure 2-8: Schematic representation of the moving boundaries formulation in the condenser.

The heat exchanger is divided in volumes equal to the number of phases of the working fluid as shown in the figure above and for each volume the mass, energy and wall energy equations are used. The length of each region changes as the working conditions change, which is taken account by means of the Leibnitz's Rule. As a result, for a 3 phase heat exchanger the following governing equations may be used:

Eq. 2-14

$$\frac{N}{2}\cdot A_c\left[\frac{dL_{SH}}{dt}(\rho_{SH}-\rho_v)+L_{SH}\frac{d\rho_{SH}}{dt}\right]+\dot{m}_A-\dot{m}_{SU}=0\ \ (\mathbf{1})$$

$$\frac{N}{2}A_cL_{SH}\left(\rho_{SH}\frac{dh_{SH}}{dt}+h_{SH}\frac{d\rho_{SH}}{dt}-\frac{dp}{dt}+\frac{dL_{SH}}{dt}(\rho_{SH}h_{SH}-\rho_vh_v)\right)=Q_{SH}+m_{su}h_{su}-m_Ah_A\ \ (\mathbf{2})$$

$$\frac{c_wM_w}{L}\left(\frac{dT_{wSH}}{dt}L_A+(T_{wSH}-T_A)\frac{dL_{SH}}{dt}\right)=\dot{Q}_{sf,SH}-\dot{Q}_{SH}\ \ (\mathbf{3})$$

$$\frac{N}{2}A_cL_{TP}\left[\frac{d\rho_v}{dP}\gamma+\frac{d\rho_l}{dP}(1-\gamma)\right]\frac{dP}{dt}+\frac{N}{2}A_c\left[\frac{dL_{TP}}{dt}(\rho_{TP}-\rho_l)+\frac{dL_{SH}}{dt}(\rho_v-\rho_l)\right]=\dot{m}_A-\dot{m}_B\ (\mathbf{4})$$

$$\frac{N}{2}A_c\left[L_{TP}\left[\gamma\left(\frac{d\rho_v}{dp}h_v+\rho_v\frac{dh_v}{dp}\right)+(1-\gamma)\left(\frac{d\rho_l}{dp}h_l+\rho_l\frac{dh_l}{dp}\right)\right]+(\rho_{TP}h_{TP}-\rho_lh_l)\frac{dL_{TP}}{dt}+(\rho_vh_v-\rho_lh_l)\frac{dL_{SH}}{dt}-L_{TP}\frac{dp}{dt}\right]=\dot{m}_Ah_v-\dot{m}_Bh_l+Q_{TP}\ (\mathbf{5})$$

$$\frac{c_wM_w}{L}\left[L_{TP}\frac{dT_{wTP}}{dt}+(T_{wA}-T_{wB})\frac{dL_{SH}}{dt}+(T_{wTP}-T_{wB})\frac{dL_{TP}}{dt}\right]=\dot{Q}_{sf,TP}-\dot{Q}_{TP}\ \ (\mathbf{6})$$

$$\frac{N}{2}\cdot A_c\left[\left(\frac{dL_{TP}}{dt}+\frac{dL_{SH}}{dt}\right)(\rho_l-\rho_{SB})+L_{SB}\frac{d\rho_{SH}}{dt}\right]+\dot{m}_{EX}-\dot{m}_B=0\ \ (\mathbf{7})$$

$$\frac{N}{2}A_cL_{SB}\left[\rho_{SB}\frac{dh_{SB}}{dt}+h_{SB}\frac{d\rho_{SB}}{dt}-\frac{dp}{dt}+\left(\frac{dL_{TP}}{dt}+\frac{dL_{SH}}{dt}\right)(\rho_lh_l-\rho_{SB}h_{SB})\right]=Q_{SB}+m_Bh_l-m_{EX}h_{EX}(\mathbf{8})$$

$$\frac{c_wM_w}{L}\left[\frac{dT_{wSB}}{dt}L_{SB}+(T_{wB}-T_{wSB})\left(\frac{dL_{SH}}{dt}+\frac{dL_{TP}}{dt}\right)\right]=\dot{Q}_{sf,SB}-\dot{Q}_{SB}\ \ (\mathbf{9})$$

where N is the number of plates of the heat exchanger and A_c the cross sectional area of the channel between two sequential plates, M_w, c_w the total mass and specific heat capacity of the

wall and L the total length of the heat exchanger, which are parameters of the model. Besides the l and v subscripts represent the saturated liquid and vapor states respectively. The rest of the variables follow the annotation given in Table 2-2.

In the above equations the time derivative of the density is expressed as a function of the time derivatives of enthalpy and pressure in each cell. For example, in cell 1 the above equation becomes:

$$\frac{d\rho_{SH}}{dt} = \left[\left(\frac{\partial \rho_{SH}}{\partial p}\right)_h + \frac{1}{2}\left(\frac{\partial \rho_{SH}}{\partial h}\right)_p \frac{dh_v}{dp}\right]\frac{dp}{dt} + \frac{1}{2}\left(\frac{\partial \rho_{SH}}{\partial h}\right)_p \frac{dh_{SU}}{dt} \quad \text{Eq. 2-15}$$

In addition, the boundary equation for each volume's length is used:

$$L_{SH} + L_{TP} + L_{SB} = L \quad \text{Eq. 2-16}$$

so 9 state variables are to be calculated: $L_{SH}, L_{TP}, h_{SH}, h_{TP}, h_{SB}, p, T_{wSH}, T_{wTP}, T_{wSB}$.

As mentioned above, the heat fluxes between the two fluid streams are calculated using the ε-NTU method. For example, Q_{SH} is calculated using the following approach:

$$\dot{Q}_{SH} = c_{p,SH}\frac{\dot{m}_A + \dot{m}_{SU}}{2}\varepsilon(T_{wSH} - T_{SU}) \quad \text{Eq. 2-17}$$

Where ε can approximately calculated using the expression for the infinity heat capacity

$$\varepsilon = 1 - e^{-NTU_{SH}} \quad \text{Eq. 2-18}$$

And

$$NTU_{SH} = \frac{U_{SH}A_{SH}}{c_{p,SH}\frac{\dot{m}_A + \dot{m}_{SU}}{2}} \quad \text{Eq. 2-19}$$

Where U_{SH} is the heat transfer coefficient for the superheated zone. In both streams the heat transfer coefficients depend on the flow rate, in compliance to the ThermoCycle MassFlowDependence heat transfer model, [3] using the following generic expression:

$$U = U_{nom}\left(\frac{\dot{m}}{\dot{m}_{nom}}\right)^{0.8} \quad \text{Eq. 2-20}$$

where the subscript nom corresponds to the nominal conditions while U_{nom}, $\dot{m}_{nom}$ are parameters of the model.

The following table summarizes the parameters selected for both heat exchangers. The geometrical data are based on the manufacturer's datasheet (SWEP F80H series) and on estimations. The nominal heat transfer coefficient values were estimated using the Dittus-Boelter correlation for single phase flow, Yan and Lin correlation for evaporation and the Kuo, Lie, Hsieh and Lin correlation for condensation [14].

Table 2-2: Heat exchanger models' parameters.

Parameter	Description	Value		Source
		Evaporator	Condenser	
N	Number of plates	50	60	Manufacturer
$A_c(m^2)$	Cross sectional area of a channel	1.96E-04	1.96E-04	Estimated
f	Enlargement factor	1.2	1.2	Estimated
$L\ (m)$	Total length of a plate	0.096	0.096	Manufacturer
$L_w\ (m)$	Effective width of a plate	0.47	0.47	Manufacturer
$M_w\ (kg)$	Total wall mass	12	16	Manufacturer
$c_w\ (J/kgK)$	Wall specific heat capacity	490	490	Manufacturer
$\dot{m}_{nom}\ (kg/s)$	Nominal flow rate for the regiregerant side	0.078	0.078	Estimated
$\dot{m}_{sf,nom}\ (kg/s)$	Nominal flow rate for the water side	0.63	0.78	Manufacturer
$U_{SH,nom}\ (W/m^2K)$	Nominal heat transfer coef in superheated region	270	265	Estimated
$U_{TP,nom}\ (W/m^2K)$	Nominal heat transfer coef in two phase region	6000	900	Estimated
$U_{SB,nom}\ (W/m^2K)$	Nominal heat transfer coef in subcooled region	-	280	Estimated
$U_{sf,nom}\ (W/m^2K)$	Nominal heat transfer coef for water	4300	5000	Estimated
γ	Mean Void Fraction	0.96	0.8	Estimated

The fixed value of the mean void fraction for both heat exchangers was calculated for the nominal conditions using the homogeneous definition (Butterworth, 1975), so:

$$\gamma = \int_{x_0}^{x_L} \frac{\frac{x}{\rho_v}}{\frac{x}{\rho_v} + \frac{1-x}{\rho_l}} dx \qquad \text{Eq. 2-21}$$

2.2.2.2 Compressor Model

In literature it is quite common to neglect the dynamics of compression/expansion machines since they tend to be much faster compared to the heat exchangers dynamics [15]. As a result, a steady state model, based on the volumetric and isentropic efficiency was used. This model is derived from the standard compressor model included in ThermoCycle library, while the volumetric and isentropic efficiencies are calculated as functions of the pressure ratio r_p [16] instead of having fixed values.

The volumetric efficiency expression has the following form:

$$e_{vol} = 1 - C\left(r_p^{\frac{1}{n}} - 1\right) \qquad \text{Eq. 2-22}$$

which is quite common for piston compressors, while the isentropic efficiency was estimated using the following equation:

$$e_{is} = K\left(1 - e^{-b \cdot r_p}\right) \qquad \text{Eq. 2-23}$$

In both equations, C, n, K and b are constants which must be calibrated to manufacturer efficiency curves. Utilizing data provided by Daikin Greece, the following values were found:

Table 2-3: Values provided by Daikin Greece.

$\boldsymbol{C}$	0.03
$\boldsymbol{n}$	1.14
$\boldsymbol{K}$	0.8454
$\boldsymbol{b}$	0.0465

As a result, the mass flow rate transferred by the compressor is calculated using the following equation:

$$\dot{m}_f = e_{vol} \frac{N_{rot}(RPM) \cdot V_s \cdot \rho_{SU}}{60} \quad \text{Eq. 2-24}$$

Where V_s the swept volume of the compressor, which is the only parameter of the model and was given by the manufacturer as $V_s = 102 \cdot 10^{-6}\ m^3$.

The enthalpy at the outlet of the compressor using the definition of the isentropic efficiency:

$$h_{ex} = h_{su} + \frac{(h_{ex,is} - h_{su})}{e_{is}} \quad \text{Eq. 2-25}$$

The shaft power needed for the compression is calculated as:

$$P_{shaft} = \dot{m}_f (h_{ex} - h_{su}) \quad \text{Eq. 2-26}$$

In order to calculate the electrical consumption P_{el} of the compressor, a simple model for the motor was included, based on the ThermoCycle ElectricDrive model. This model is using just a constant value for the efficiency of the electromechanical power conversion, which was assumed as:

$$\eta_m = \frac{P_{shaft}}{P_{el}} = 0.93 \quad \text{Eq. 2-27}$$

Besides, the model was modified in order to take account of the electromechanical slip of an induction motor, which is an extra parameter of the model, defined as:

$$s = \frac{N_{rot,s} - N_{rot}}{N_{rot,s}} \quad \text{Eq. 2-28}$$

Where $N_{rot,s}$ is the synchronous speed. Since the motor has 4 poles, the synchronous speed in a common 50 Hz grid is $N_{rot,s} = 1500\ RPM$.

2.2.2.3 Thermostatic expansion valve (TEXV) model

The thermostatic expansion valve model is based on the standard valve component of the ThermoCycle library, controlled by a PID controller which maintains the superheating at a

desired value. While this implementation is actually an Electronic Expansion Valve (EEV) its operation is similar to the standard TEXV's operation.

The mass flow rate through the valve is calculated form the pressure drop using the following expression:

$$\dot{m}_f = A \cdot \sqrt{2 \cdot \rho_{SU} \cdot \Delta p} \quad \text{Eq. 2-29}$$

where A is the area of the orifice inside the valve. A is changing linearly with the control signal, so:

$$A = y \cdot A_{full} \quad \text{Eq. 2-30}$$

The fluid flow through the valve is assumed adiabatic, so the expansion is isenthalpic:

$$h_{SU} = h_{EX} \quad \text{Eq. 2-31}$$

The superheating of the fluid exiting the evaporator is calculated in "real time" by measuring its pressure and temperature using the SensTp component from ThermoCycle. In order to calculate the degree of superheating the saturation temperature of the R410A was fitted against the saturation pressure with a 6th order polynomial, just like a "real world" implementation of such a controller.

The gains of the PID controller were set empirically in order to achieve a fast but smooth operation and avoid oscillations that avoid the robustness of the model. The values used are given in the following table:

Table 2-4: PID controller values.

K	-0.6
T_i	2
T_d	0.3

2.2.2.4 Pressure drop components

In order to take account of the pressure drop in both the refrigerant and water loops (since the pressure drop inside the heat exchangers is neglected), a pressure drop component was used, which is governed by the following equation:

$$\dot{m}_f = K\sqrt{\Delta p} \quad \text{Eq. 2-32}$$

K is calculated from the nominal conditions of each stream, which are given by the manufacturer for the water loops and are assumed to be 0.1 bar at 0.078 kg/s for the refrigerant side of each heat exchanger.

2.2.2.5 Three-way valves

Since the heat pump does not include a 4-way valve in order to revert from cooling to heating mode, the only way to operate it during winter is to swap the hydraulic connections. This swapping was implemented with four 3-way valve components, which are developed using two standard valve components from ThermoCycle. Two different variants of this model where developed, the diverting valve, having 1 inlet and 2 outlets, and the mixing valve, having 2 inlets and 1 outlet. In both cases, when the first 2way valve is fully opened, the second is fully closed, so if the signal controlling the first valve is y, the signal for the second valve is 1-y.

2.2.2.6 The heat pump model

The following picture shows the component diagram of the whole heat pump model in the Dymola environment. The next picture depicts a model of the heat pump including the 3way valves, which are used to revert from cooling to heating mode.

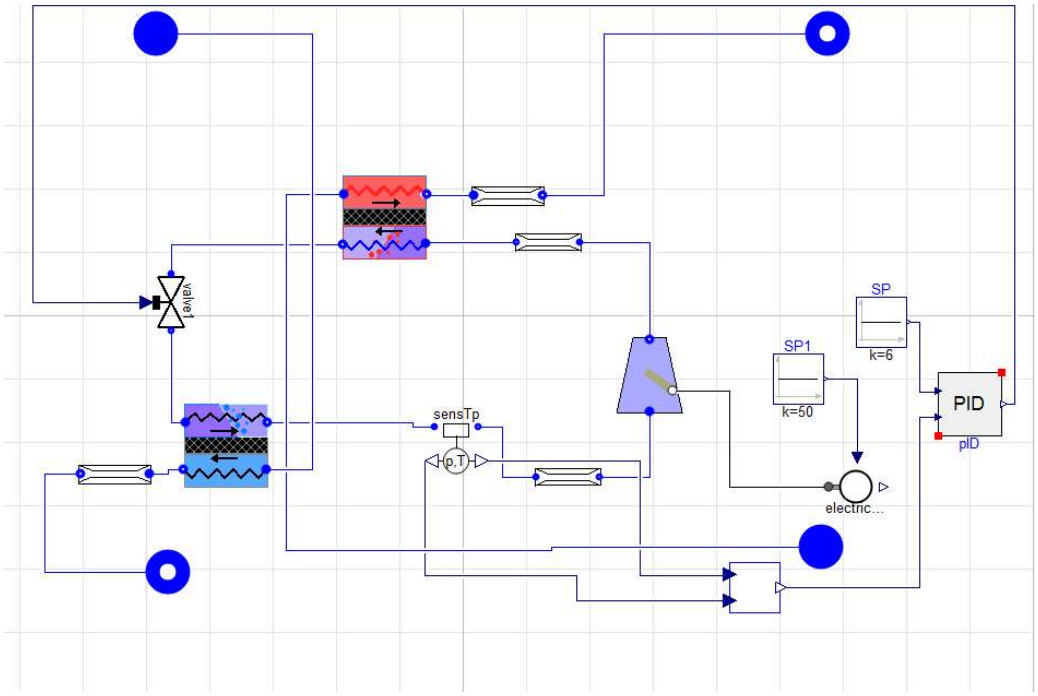

Figure 2-9: Schematic of the heat pump model in the Dymola environment.

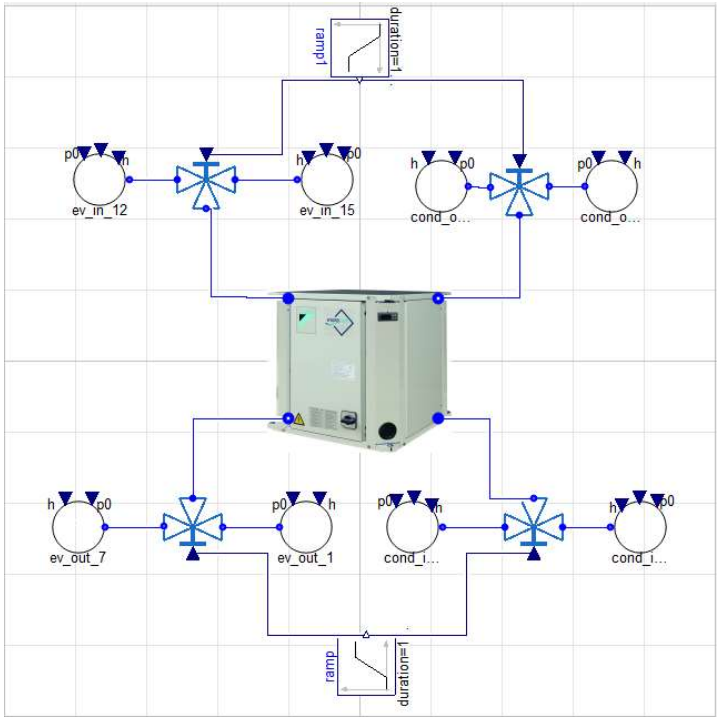

Figure 2-10: Schematic of the heat pump among the four 3-way valves for operation switching.

2.2.3 Typical example

In order to test the heat pump model, the following scenario was run:

1. For t=0-250s the heat pump works on its nominal conditions as a chiller.
2. For t=250-300s the water flow through the evaporator linearly decreases till the 60% of its nominal value.
3. At t=500s the machine is reverted to heat pump operation, and the water boundary conditions are reverted to the corresponding nominal point.

The following Figure 2-11 depicts the response of the evaporator and condenser thermal power during the test:

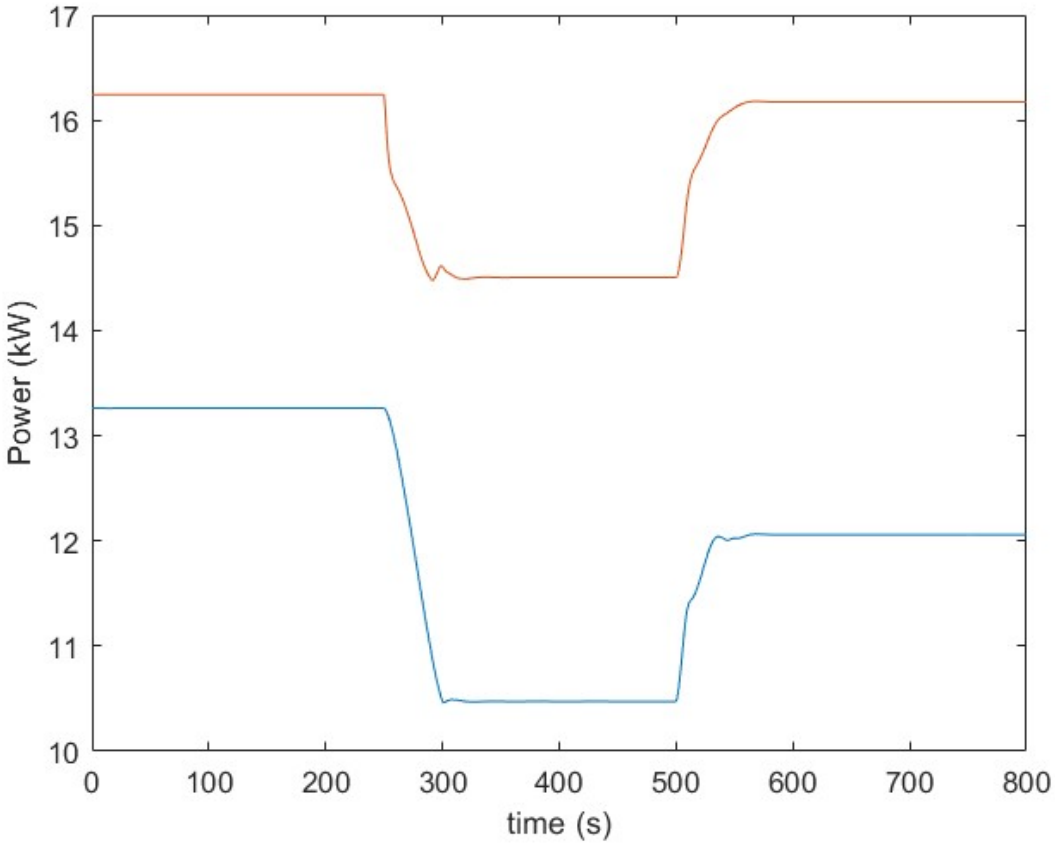

Figure 2-11: Condenser and evaporator capacities during the test.

In addition, the response of the control signal of the TEXV and the evaporation pressure during the cooling load decrease is summarized in the following Figure 2-12:

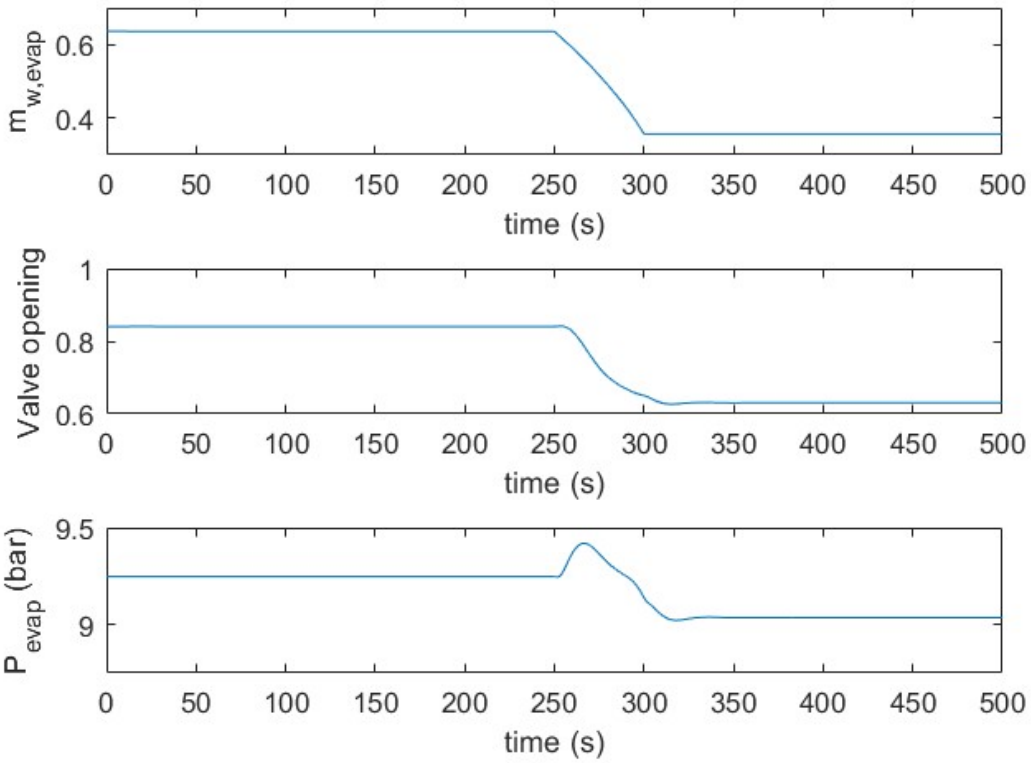

Figure 2-12: Response of the TEXV during the evaporator load change.

Finally, the results of the model were compared against performance data provided by Daikin Greece, for various evaporator capacities in either heat pump or chiller mode. The following chart shows that the relative error between the model results in steady state and the performance tables is in major below the ±5% limit for both the evaporator capacity and the electrical Coefficient Of Performance (COP).

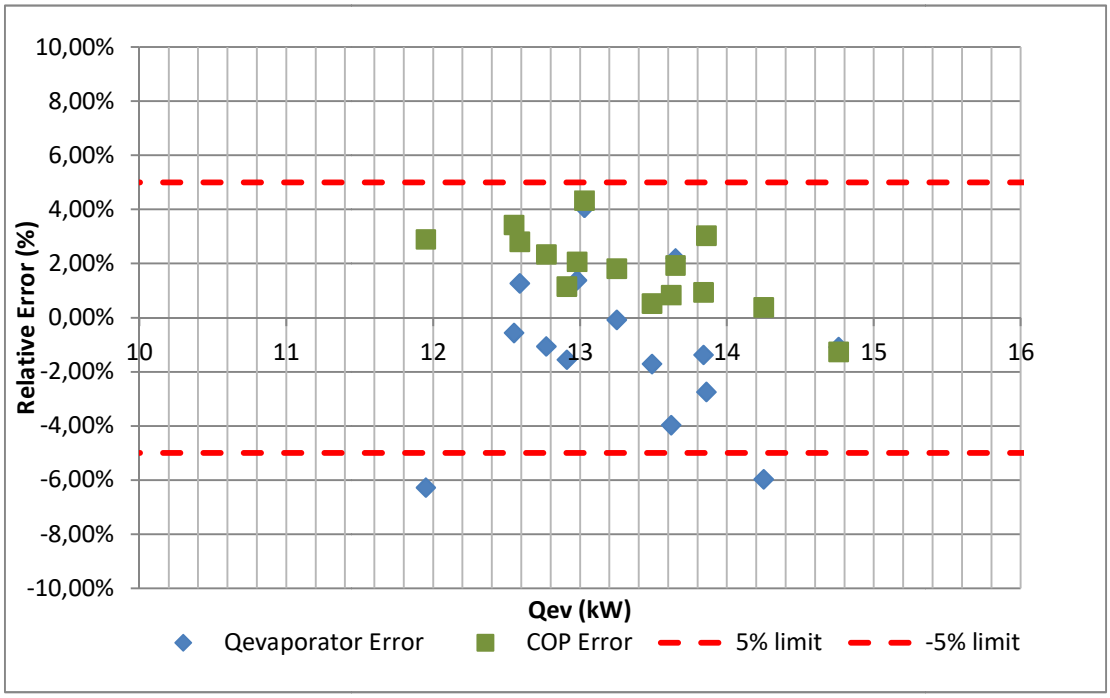

Figure 2-13: Comparison of the model results to Daikin performance table for various evaporator capacities.

2.2.4 Interface to the hybrid subsystem model

The heat pump model can be directly connected to other components developed in Dymola using the ThermoCycle library via the standard FlangeA and FlangeB fluid ports. The interconnection with the adsorption module can be done hydraulically, while the Refrigerant-PCM-Water heat exchanger should be integrated inside the refrigerant loop, leading to the creation of a new heat pump model. Finally, the frequency of the compressor can be controlled through an external input connector, in order to control the start-up and shutdown mode of the heat pump, while the electrical consumption of the compressor is available to the battery model via a real output connector.

2.3 Continental outdoor unit (Air side evaporator and fan module) (AIT)

2.3.1 Introduction

In the Continental system, a finned tube air source HEX will be used as an evaporator to extract renewable heat from air. Today, Modelica models of air source HEX exist in several libraries like in the free Thermocycle-Library [17] or in the commercial TIL-Suite library [18]. Unfortunately, none of these libraries consider the frost aggregation during operation in winter. Therefore, we extended an existing discrete cross-flow HEX from the open source ThermocycleLibrary (CrossHX) to consider also frost aggregation of the HEX, for realistic simulations of the Continental system during winter (→ FrostCrossHX). The refrigerant side of the HEX was not changed and therefore, a good integration into the existing library can be expected. The air side was completely rewritten for a finned tube HEX and furthermore, a fan attached to the HEX was introduced into the model. Because no further connections on the air side are expected. The air sources and sinks were also integrated into the new FrostCrossHX component.

Figure 2-14 shows a finned tube HEX from the front at different points of time during operation at 2°C on the air side and at about -7°C on the refrigerant side. After about one hour of operation, the complete HEX is covered with frost and the COP of the heat pump has decreased from 3 to 2.6.

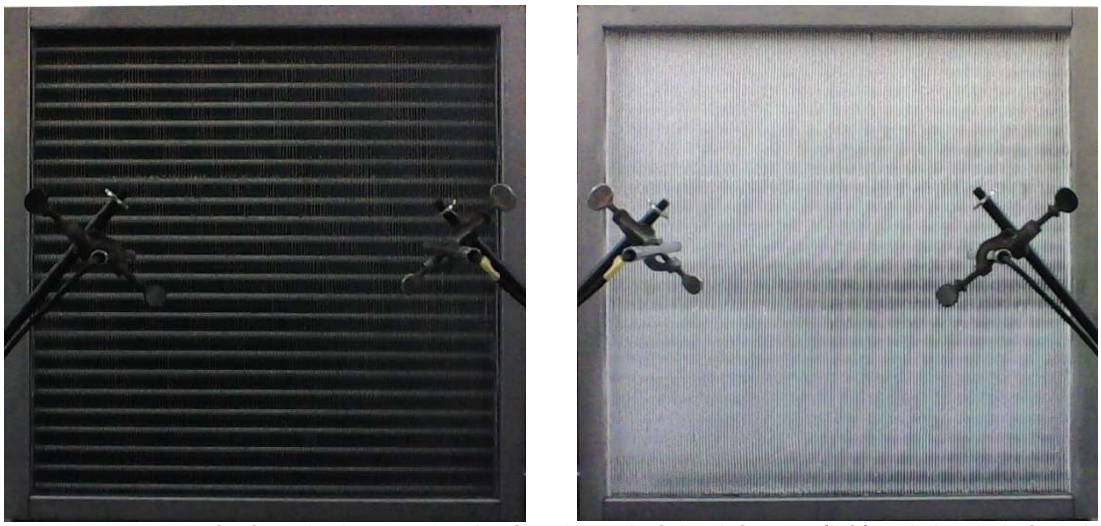

Figure 2-14: Image of a finned tube HEX shortly after the end of the defrosting (left) and shortly before the start of the defrosting (right). The images were taken during an experiment of a previous project at AIT (SilentAirHP [19]).

2.3.2 Methodology

To describe a three-dimensional finned tube HEX in a 1D-Model we have to make a few assumptions:

- Fins and tubes of the HEX will be described as a cold wall with a constant temperature on their surface.
- The latent heat of condensation or desublimation, respectively, dissipates solely on the frost surface and in the frost layer.
- The heat transfer coefficient is calculated from a Nusselt-number, which for its part is calculated from analytical equations for finned tube HEX found in literature. The influence of the roughness of the frost surface was not considered.
- The mass transfer coefficient is calculated from the Lewis relationship with $Le^{2/3}$=0.9.
- The temperature and humidity distribution in the frost layer is calculated analytically by assuming quasi-static conditions inside the layer.
- The frost layer thickness z_{fs} and the density of the frost layer ϱ_f are state variables of the problem. As fixed initial values we use z_{fs}=2 x 10^{-5} m and ϱ_f = 30 kg/m^3, respectively.
- The thermal conductivity of the frost layer depends on the frost density.
- The pressure loss was calculated analytically with equations from literature considering the dimensions of the HEX and the increasing frost thickness.

Figure 2-15 shows a symmetry cell of the FrostCrossHX used to calculate the pressure loss and the Nu-number (a) and the mathematical one-dimensional cell to describe the problem (b). The model of the refrigerant and the cold wall is similar to the CrossHX from the Thermocycle-Library, but the area of the fins is calculated from input parameters of the FrostCrossHX. Once the temperature of the fin is below the dew point temperature of the incoming air ϑ_a^{in} and depending if the wall temperature is below 0°C, water will condensate or desublimate on the wall, respectively. In the following, we will only describe the modeling of the frosting process, which is the more complex one, in detail.

Once frost aggregation has started, two mechanisms can be observed. On the one hand, the frost layer grows which is described with an increasing frost thickness z_{fs} and a mass flow of water vapor that desublimates on the free surface of the frost layer ($\dot{m}_g$). On the other hand, the frost layer becomes more and more dense with time because of diffusive mass transport of the water vapor into the frost layer ($\dot{m}_d$). The first effect, leads to a decreasing cross-section for the air and therefore, to a higher pressure loss than during frost-free operation. This affects the distribution of the mass flow through all parallel cells, as well as, the total volume flow through the HEX. Furthermore, the enhancement of the thickness of the frost layer leads to a decreasing heat transfer through the layer whereas the densification of the frost layer on the other hand increases the thermal conductivity. However, it is obvious that after a certain time, the frost layer will block the entire air channel. Long time before this happens, the heat pump has to react and needs to switch into the defrost or reverse mode where it heats up the evaporator to melt the ice and get rid of the frost layer. Several models exist to describe this behavior [20],[21],[22],[23], [24] whereby we mainly followed the approach of [24]. Contrary to [24], we considered the fin-efficiency indirectly by adapting the heat transfer coefficients [25], we separated the specific heat capacity of air into a dry air part and a water vapor part and we considered a quadratic instead of a cubic pressure dependence of the fan.

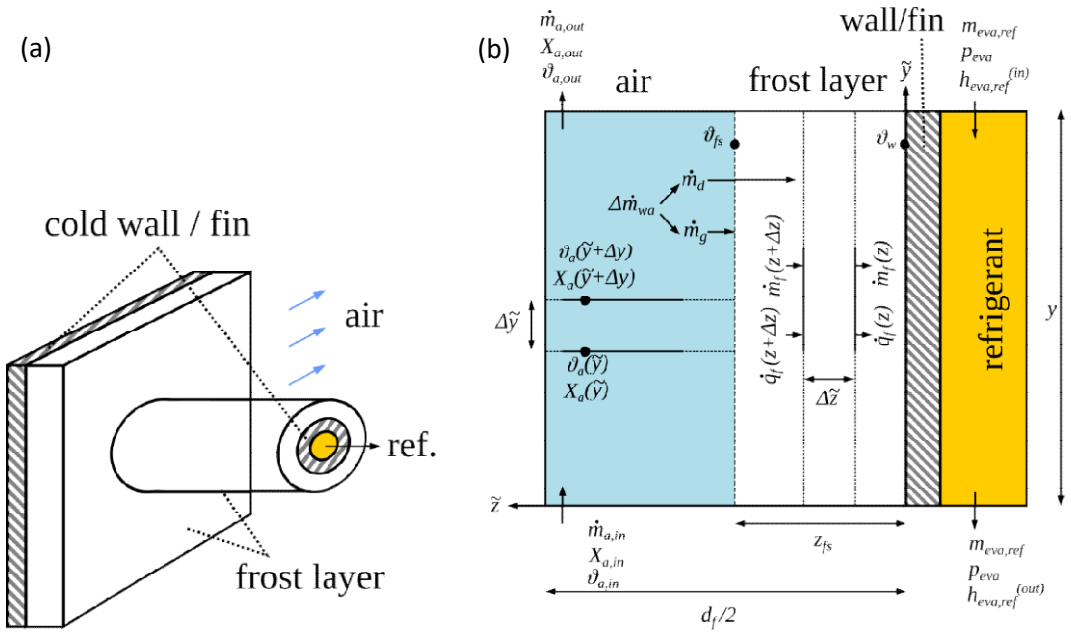

Figure 2-15: (a) Section of a symmetry cell of the finned tube HEX (FrostCrossHX) and sketch of the mathematical description of the 1-D discretized model (b). In the entire evaporator model, the air channels are arranged in parallel, whereas the refrigerant cells are connected in series (Cross-flow-arrangement).

The mass balance equations in the air cell are:

$$\dot{m}_{da}\,(\tilde{y}) - \dot{m}_{da}\,(\tilde{y} + dy) = 0 \qquad \text{Eq. 2-33}$$

$$\dot{m}_{da}\,(\tilde{y})\,\big(X(\tilde{y}) - X(\tilde{y} + dy)\big) - K_m\,A_p\,dy\,\Big(X_{fs} - X(\tilde{y})\Big) = 0 \qquad \text{Eq. 2-34}$$

Where $\dot{m}_{da}$ represents the mass flow rate of the dry air, X represents the specific humidity of the air, K_m represents the mass transfer coefficient which is calculated over the Lewis relationship from the heat transfer coefficient K_h, A_p represents the area between air and frost surface per unit length and X_{fs} is the specific humidity at the frost surface calculated from the temperature at the frost surface ϑ_{fs} by assuming saturated air conditions. The energy balance in the air cell describes the sensible heat transfer:

$$\dot{m}_{da}\,\Big(c_{p,da} + X_a^{(in)}\,c_{p,wv}\Big)\,\big(\vartheta(\tilde{y}) - \vartheta\,(\tilde{y} + dy)\big) + K_h A_p dy\,\Big(\vartheta_{fs} - \vartheta(\tilde{y})\Big) = 0 \qquad \text{Eq. 2-35}$$

where we have neglected the mass transport into the frost layer (approx. 0.5% of the total energy) for the sake of the possibility to decouple the heat and mass transfer in the air cell. Here, $c_{p,da}$ represents the specific heat capacity of dry air, $c_{p,wv}$ represents the specific heat capacity of the water vapor and $X_a^{(in)}$ represents the specific humidity of air at the inlet. Starting from (Eq. 2-34) and (Eq. 2-35) one can find after algebraic transformations, Taylor-series expansion and solving differential equations the following two equations for the mass- and sensible heat transfer:

$$\Delta\dot{m}_{wa} = \dot{m}_g + \dot{m}_d = \dot{m}_{da}\,\Big(X_a^{(in)} - X_{fs}\Big)\Big(1 - e^{-\frac{K_m A_p}{\dot{m}_{da}} y}\Big) \qquad \text{Eq. 2-36}$$

$$\dot{Q}_{a,sensible} = \dot{m}_{da}\left(c_{p,da} + X_a^{(in)}\, c_{p,wv}\right)\left(\vartheta_a^{in} - \vartheta_{fs}\right) \times\left(1 - \exp\left(-\frac{K_h A_p}{\dot{m}_{da}\left(c_{p,da} + X_a^{(in)}\, c_{p,wv}\right)}\, y\right)\right)$$ Eq. 2-37

where y represents the length of the cell, $\dot{m}_g$ is the amount of water vapor that is responsible for the growth of the frost layer and $\dot{m}_d$ is the amount of water vapor that is responsible for the densification. The water vapor diffusion into the frost layer can be calculated analytically by a quasi-static approach starting from the mass balance in the frost layer:

$$D\frac{\varepsilon}{\tau}\frac{d^2 X_f}{dz^2} = \lambda X_f$$ Eq. 2-38

Where X_f is the specific humidity in the frost layer, λ represents an absorption coefficient, D is the diffusivity of water, ε represensts the porosity and τ represents the turtuosity of the frost layer. Correlations for the latter three can be found in literature [20], [23], [24]. By solving (Eq. 2-38) analytically, and inserting the boundary conditions of the given problem, one can find an analytical solution for the absorption coefficient:

$$\lambda = D\frac{\varepsilon}{\tau}\left(\frac{1}{z_{fs}}\cosh^{-1}\left(\frac{X_{fs}}{X_w}\right)\right)^2$$ Eq. 2-39

where X_w represents the specific humidity at the wall to the refrigerant.

With (Eq. 2-39) and (Eq. 2-38) one can calculate the water vapor mass flow into the frost layer:

$$\dot{m}_d = \varrho_{da} A_p y \int_0^{z_{fs}} \lambda\, X_f(\tilde{z})\, dz = \varrho_{da} A_p y X_w \lambda \sqrt{\frac{D\varepsilon}{\lambda\tau}}\sinh\left(\sqrt{\frac{D\varepsilon}{\lambda\tau}}\, z_{fs}\right)$$ Eq. 2-40

The frost layer thickness z_{fs} and density ϱ_f are state variables and are therefore calculated numerically by the Integration solver using:

$$\frac{dz_{fs}}{dt} = \frac{\dot{m}_g}{\varrho_f A_p y}$$ Eq. 2-41

$$\frac{d\varrho_f}{dt} = \frac{\dot{m}_d}{z_{fs} A_p y}$$ Eq. 2-42

where $\dot{m}_g$ can be calculated from (Eq. 2-36) and (Eq. 2-40). For numerical reasons the minimum frost layer thickness was limited to 2 x 10^{-5} m and the minimum density was limited with 30 kg/m^3. As already mentioned, these values were also used as initial values for the simulations.

The heat transfer in the frost layer considering the latent heat from the desublimation can be described with:

$$k_f \frac{d^2\vartheta_f}{dz^2} = -\Delta h_{sv}\lambda\varrho_a X_f(\tilde{z})$$ Eq. 2-43

where k_f is the thermal conductivity and Δh_{sv} represents the specific heat of desublimation.

At the frost layer surface, the sensible heat from the air $\dot{Q}_{a,sensible}$ on the one hand, and the latent heat from the desublimation process of the frost growth ($\dot{Q}_{g,latent} = \dot{m}_g\, \Delta h_{sv}$) on the other hand is transferred to the frost layer. By applying the Fourier law at the frost surface, some algebraic transformations and considering the boundary conditions we can solve (Eq. 2-43) analytically for the temperature in the frost layer and especially at the frost surface ϑ_{fs}:

$$\vartheta_{fs} = \frac{\left(\dot{Q}_{a,sensible} + \dot{Q}_{g,latent}\right)}{A_p y\, k_f} z_{fs} + \frac{\Delta h_{sv}\, \varrho_{da} X_w D\, \varepsilon}{k_f \tau} \left(1 - \cosh\left(\sqrt{\frac{\lambda\tau}{D\varepsilon}} z_{fs}\right)\right) + \vartheta_w \qquad \text{Eq. 2-44}$$

which is needed to calculate the heat transfer between air cell and frost layer. Finally, the heat transferred to the refrigerant cell via the wall is given with:

$$\dot{Q}_w = \dot{Q}_{a,sensible} + \dot{Q}_{g,\boldsymbol{latent}} + \dot{Q}_{d,latent} = \dot{Q}_{a,sensible} + \Delta\dot{m}_{wa}\, \Delta h_{sv} \qquad \text{Eq. 2-45}$$

With (Eq. 2-33) to (Eq. 2-45) all necessary equations are given to describe the heat and mass transfer in the HEX during frosting. The increasing frost thickness changes the heat transfer on the one hand and increases the pressure drop in the HEX on the other hand. Correlations between pressure drop, heat transfer coefficients K_h and the finned tube geometry were also implemented in the model. A detailed description of the used correlations can be found in [25].

The process of defrosting is similar described as the frosting process, although different stages of defrosting have to be considered. A detailed description how to implement the defrosting process can be found in [23] and will also be implemented in the presented Modelica models.

Please note that, also condensation for temperatures above 0°C has to be considered in the present models. In this case the air is dehumidified, but no frost aggregates. We assume that the liquid water that condenses in the HEX flows away immediately in our models.

2.3.3 Auxiliary components

The Continental outdoor unit model includes also a fan which is responsible for the air flow through the evaporator. The pressure dependency of the fan is described with a quadratic law:

$$\Delta p_{\boldsymbol{fan},nom} = a_0 + a_1\, \dot{V}_{nom}^2 \qquad \text{Eq. 2-46}$$

and variations of the rotational speed form the nominal rotational speed of the fan are implemented with the aid of general fan equations:

$$\frac{\dot{V}}{\dot{V}_{nom}} = \frac{n}{n_{nom}} \qquad \text{Eq. 2-47}$$

$$\frac{\Delta p_{fan}}{\Delta p_{fan,nom}} = \left(\frac{n}{n_{nom}}\right)^2 \qquad \text{Eq. 2-48}$$

The air cells of the FrostCrossHX are arranged in parallel, therefore, the pressure drop in all cells has to be the same on the one hand side, and the fan has to provide the power to overcome the pressure drop in the HEX:

$$\Delta p_{\boldsymbol{fan}} = \Delta p_i \qquad i \in 1 \ldots n \qquad \text{Eq. 2-49}$$

where n is the amount of discretized cells in refrigerant flow direction and Δp_i is the pressure drop in each cell calculated from the geometry of the finned tube cell considering the frost layer thickness (c.f. [25]).

2.3.4 Typical example

Figure 2-16 shows the FrostCrossHX integrated in a heat pump cycle with two PID-controllers to guarantee a constant superheating after the evaporator of 3 K and a constant inlet temperature to the heating system of 37 °C. The outdoor air temperature in this example is 2 °C at 90% r.h. The FrostCrossHX was discretized with 10 cells in refrigerant direction.

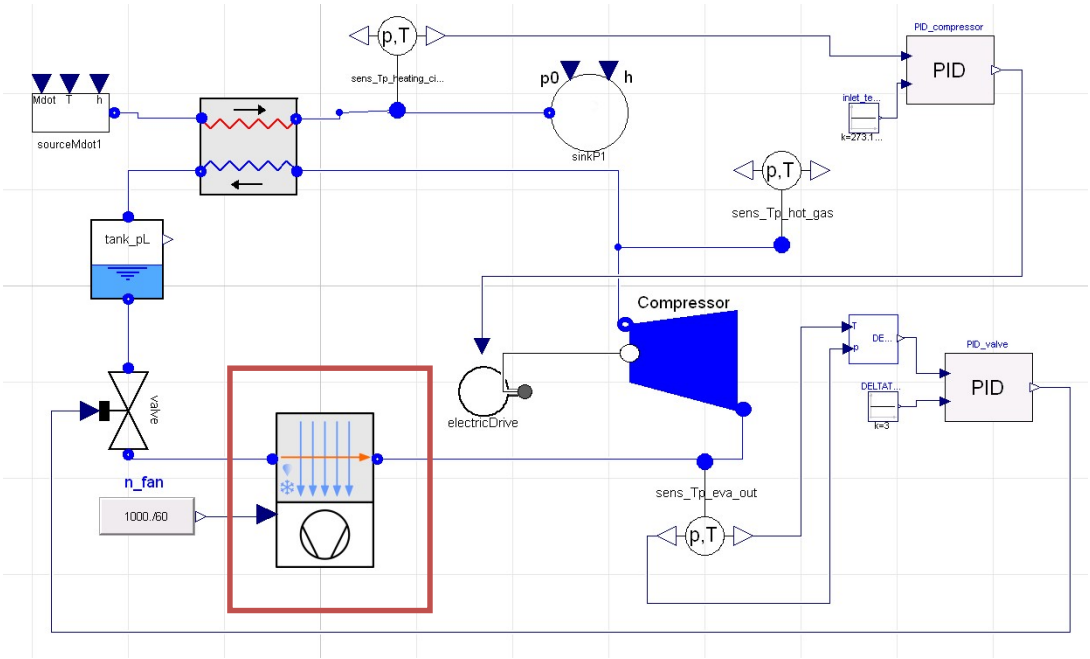

Figure 2-16: System sketch of the modelled FrostCrossHEX (red square) integrated in a heat pump cycle in Dymola/Modelica.

The heat pump was started at time = 0 s with reasonable initial conditions. Figure 2-17 show how the FrostCrossHEX behaves after starting the compressor in each cell. The frost thickness z_{fs} increases with time because ice aggregates at the fins and tubes on the air side of the evaporator (c.f. left subfigure in Figure 2-17). Contrary to cell 1-9, the frost thickness in the last cell (cell 10) does not increase from the beginning. The reason becomes obvious if one looks at right subfigure in Figure 2-17. The temperature of the wall (frost surface) in the last cell is still slightly above 0°C, hence liquid water condensates and flows away instead of frost aggregation. The temperature in the first nine cells is quite similar because of the small temperature glide in R32 whereas the refrigerant is in the vapor phase in the last cell (low heat transfer) and the PID controller (PID_valve) ensures, that the outlet temperature of the refrigerant is above the saturation temperature (superheating). All temperatures decrease with time in Figure 2-17, due to the fact, that the heat transfer over the increasing frost layer (increased thermal resistance) has to be maintained by an increasing temperature difference between the refrigerant and air. Due to the free passage for the air in cell 10 (no frost aggregation) the volume flow redistributes (see left subfigure of Figure 2-18). Whilst the volume flow in the frost cells decreases, the volume flow in the frost-free cell increases first. After about 4000s, the refrigerant temperature in the evaporator needed to be lowered so

much (due to the increased thermal resistance in cell 1 to 9), that the temperature in cell 10 drops below the freezing point, too. Hence, frost aggregation starts also after about 4000s in cell 10 (see left subfigure of Figure 2-17).

Along with the decreasing cross-sections, the overall pressure drop increases if a constant rotational speed of the fan is assumed, also the total volume flow over the HEX decreases with time.

Note that the PID controller (PID_compressor) ensures in the described system that the heat transferred to the heating system stays constant and therefore it lowers the pressure (and therefore the temperature) in the evaporator until enough heat is extracted from the air to the refrigerant. Because of the lower temperature in the evaporator, also the COP of the system decreases with increasing frost thickness. In the given example the overall COP decreases from about 3.5 to 3.3 during 2 hours of operation due to the increasing power consumption of the fan and the compressor.

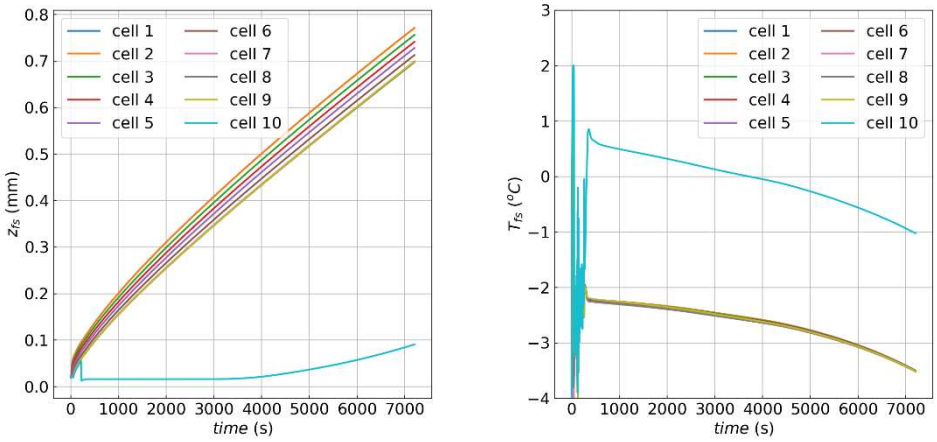

Figure 2-17: Ice aggregation in the evaporator (left) and temperature at the frost surface (right)

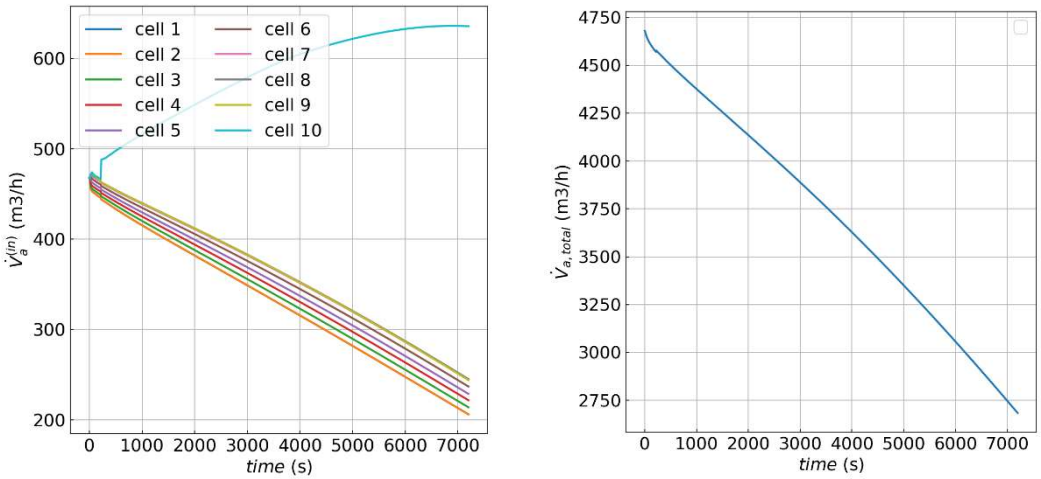

Figure 2-18: Redistribution of the air volume flow in each cell (left) and change of the total air volume flow rate (right)

2.3.5 Interface to the hybrid subsystem model

The FrostCrossHEX is connected with its refrigerant (fluid) inlet and outlet and a Real input for the fan speed to the outside world. Standard ports from the ThermoCycle and the Modelica Standard Library are used to realize these connections. Fan, air source and sink are implemented in the FrostCrossHEX-model; hence, the airside does not need to be connected to the outside.

2.4 RPW-HEX module for Mediterranean and Continental concept (UDL - RPW-HEX modelling, AIT - Modelica implementation and PCM property modelling)

2.4.1 Introduction

Figure 2-19 shows the general operating conditions and a modeling scheme of the RPW-HEX module for the Mediterranean concept. The model developed will calculate the refrigerant conditions at the outlet (point 1) of the HEX while the state of charge of the PCM will be also calculated. In order to run, the model needs the refrigerant characteristics at the inlet of the HEX (point 4). Pressure and volume flow rate is the same in point 4 and point 1.

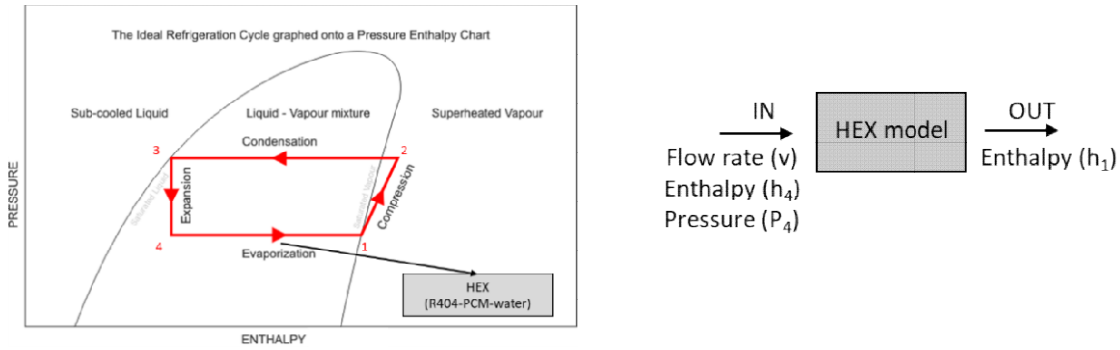

Figure 2-19: Scheme of the vapour-compression cycle in a pressure-enthalpy curve (MED system), the section where the RPW HEX is used and a schematic view of the RPW HEX model.

2.4.2 Methodology – modeling approach

Figure 2-20 shows a scheme of the 3-fluid (refrigerant, water and PCM) heat exchanger built at AKG facilities, which will be sent to UDL in order to experimentally study its behaviour. In order to further study its behaviour a numerical model is also developed. Figure 2-21 shows the proposed 2D numerical model, which considers solely one refrigerant + water + PCM layer. The discretization of each of the control volume is shown in Figure 2-22. Notice that there are 3 possible working conditions in the Mediterranean concept:

- Refrigerant is charging the PCM (Figure 2-22-left). There is no water circulation.
- Water is discharging the PCM (Figure 2-22-centre). There is no refrigerant circulation.
- Refrigerant cooling the water (Figure 2-22-right). In this situation the PCM will be partially charged.

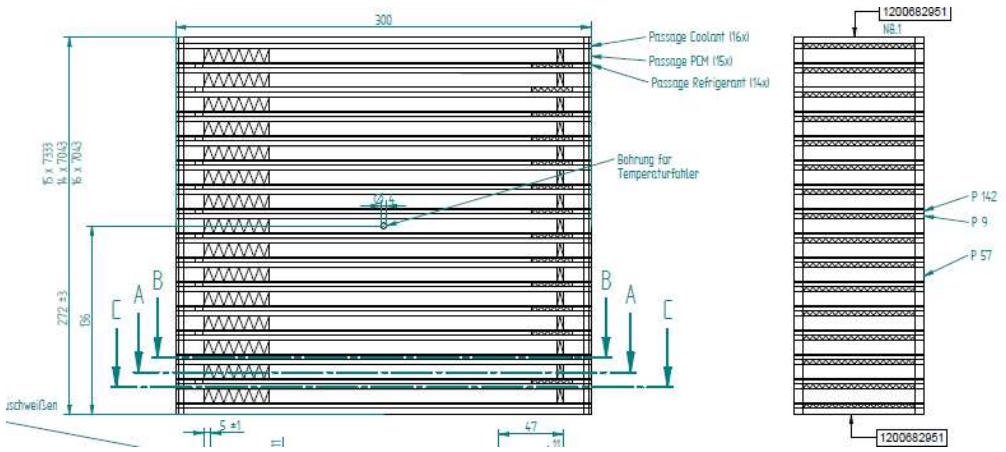

Figure 2-20: Scheme of the 3-fluid HEX build at AKG.

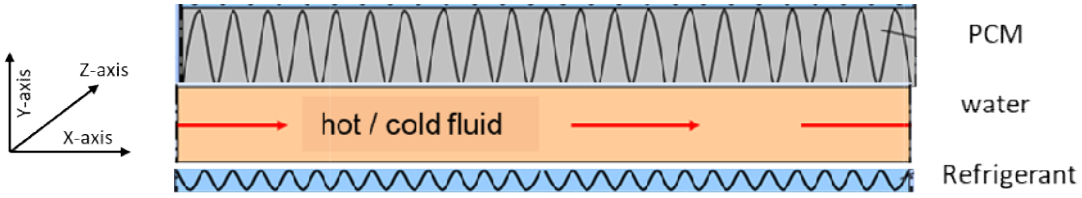

Figure 2-21: Scheme of the control volume assumed for the simulation.

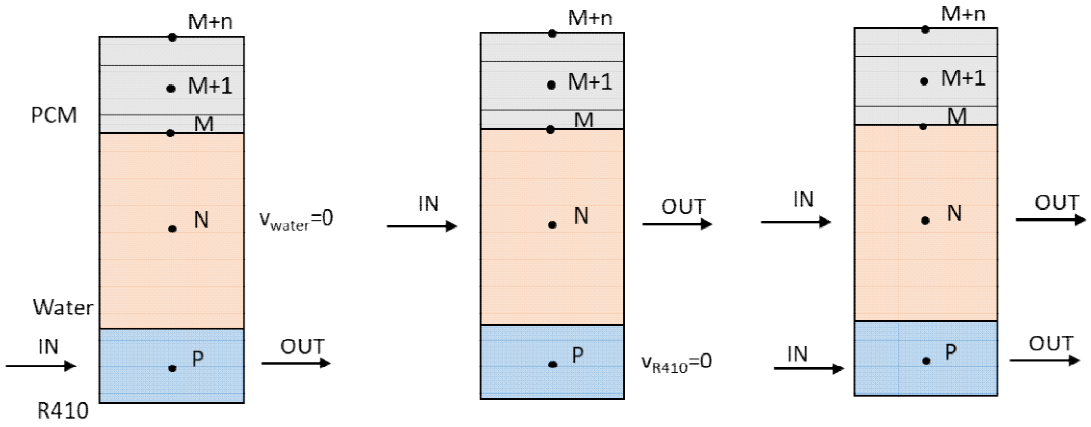

Figure 2-22: Scheme of the discretization of the control volume assumed for three different scenarios: left: PCM charging, centre: PCM discharging, right: standard working conditions.

The two-dimensional heat transfer during charging/discharging is governed by the following equation:

$$\sum \dot{Q} + (\dot{m}_{in} \cdot h_{in}) - (\dot{m}_{out} \cdot h_{out}) = \rho \cdot C_p \cdot \frac{\Delta T}{\Delta t} \cdot dV \qquad \text{Eq. 2-50}$$

The governing equation is completed by the following initial and boundary conditions:

- In a charging process (refrigerant is cooling PCM), the velocity of water is 0. $V_{water} = 0$.
- In a discharging process (water is cooled by the PCM), the velocity of refrigerant is 0. $V_{refrigerant} = 0$.
- No convection in the liquid phase of the PCM due to small space.
- The material of the HEX (aluminium) is not considered in the heat transfer analysis.
- The refrigerant (node P) is in contact with the PCM (node M+n).
- There is no heat transfer to the surrounding.
- The PCM is homogeneous and isotropic.
- The latent heat effect of PCM is addressed using effective heat capacity as function of temperature.

The system of algebraic equations is obtained by discretizing the Eq. 2-50 over each control volume (Figure 2-23).

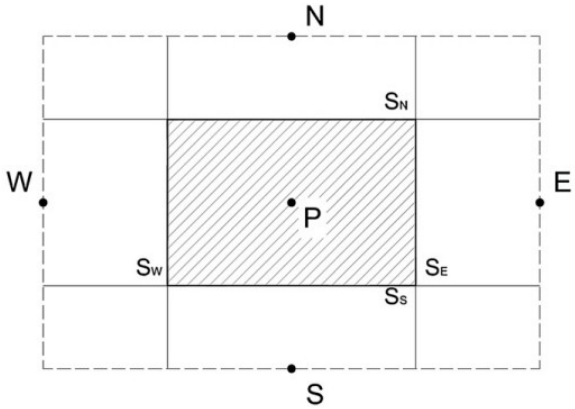

Figure 2-23: Two-dimensional domain used in the discretization of the system.

In the model the number of nodes taken in x-direction were 100 nodes, for the y-direction solely one node is used for the refrigerant and water respectively while 5 nodes were considered for PCM. The system of algebraic linear equations extracted from the finite volume method was solved using Gauss Seidel iterative method with a time step of 1 second. The solution was found to be mesh-independent based on the above nodes selection.

2.4.3 Refrigerant control volume

On one hand, when the refrigerant is boiling the temperature is constant at the saturated temperature ($T_P = T_{sat,P}$) and the enthalpy is changing. On the other hand, when the refrigerant is in vapour phase the temperature changes over time. In this situation, $h=C_p \cdot T$ in Eq. 2-51. While in a charging process: $\dot{m}_{in} = \dot{m}_{out}$, in a discharging process $\dot{m}_{in} = \dot{m}_{\boldsymbol{out}} = 0$.

$$\dot{Q}_{conv,M+n} - \dot{Q}_{conv,N} + \dot{Q}_{\boldsymbol{cond},P-1} - \dot{Q}_{cond,P+1} + (\dot{m}_{in} \cdot h_{in}) - (\dot{m}_{out} \cdot h_{out}) = \rho \cdot \frac{(h_P^{t+1} - h_P^t)}{\Delta t} \cdot dV \qquad \text{Eq. 2-51}$$

The physical situation occurring in two-phase heating/cooling process is more complicated and, consequently, the correlations for estimating flow-boiling and flow-condensation heat transfer coefficients are also more complicated. These correlations are almost always based on fitting some set of measurements rather than a complete model of the physical situation. Therefore, the predicted heat transfer coefficient also has larger uncertainty bands,

particularly when the correlations are applied outside of the range of conditions associated with the data.

There have been literally hundreds of correlations proposed for flow boiling/condensation heat transfer coefficient. A review of the most well-accepted correlations for boiling (occurring in the evaporator) has been prepared by Shah [26], concluding that the correlation proposed by Shah [27], [28] provides the most consistent agreement with the available experimental data, with a mean deviation of less than 20%. However, some researchers have focused on evaluating the convective boiling heat transfer coefficients for R410A, and in particular in microchannel. Yun et al. [29] concluded that the boiling heat transfer coefficients of R410A in microchannel are much higher than existing data for single tubes at similar test conditions, and the effects of tests conditions (in particular the effects of saturation temperature, mass flux, and heat flux) on the heat transfer coefficients are relatively small. The pressure drop of R410A in microchannel shows very similar trends with those in large diameter tubes. A correlation for the heat transfer coefficients (h) in microchannel is proposed by considering heat transfer mechanisms in small diameter tubes, as shown in Eq. 2-52.

$$h = 13687 \cdot (Bo \cdot We_l)^{0.1993} \cdot Re_l^{-0.1626} \quad \text{Eq. 2-52}$$

where We is the Weber number, defined for Eq. 2-53

$$We = \frac{\rho \cdot v^2 \cdot l}{\sigma} \quad \text{Eq. 2-53}$$

where ρ is the density of the fluid, v is the velocity, l is the characteristic length, typically the droplet diameter, and σ is the surface tension.

$$Re_l = \frac{G \cdot (1 - x) \cdot D_h}{\mu_{l,sat}} \quad \text{Eq. 2-54}$$

where Bo can also be calculated as:

$$Bo = h \cdot \frac{T_w - T_{ref}}{\rho \cdot u \cdot (h_g - h_f)} \quad \text{Eq. 2-55}$$

where T_w is the wall temperature, T_{ref} is the refrigerant temperature, ρ is the density of the refrigerant, u is the refrigerant velocity, h_g is the enthalpy of saturated vapour and h_f is the enthalpy of saturated liquid.

The problem is that in order to calculate Bo, the heat transfer coefficient, h, must also be known. But with proper mathematical formulation, h can be isolated as follows. From Eq. 2-52:

$$\text{if } A = 13687 \cdot We_l^{0.1993} \cdot Re_l^{-0.1626} \text{ and n = 0.1993} \quad \text{Eq. 2-56}$$

$$h = A \cdot Bo^n$$

$$\text{if } Bo = h \cdot B \text{ where } B = \frac{T_w - T_{ref}}{\rho \cdot u \cdot (h_g - h_f)} \quad \text{Eq. 2-57}$$

$h = A \cdot (h \cdot B)^n$ thus, $h = A \cdot B^n \cdot h^n$

$$\text{if } K = A \cdot B^n \qquad \text{Eq. 2-58}$$

$$h = K \cdot h^n$$

Eq. 2-58 can be solved by:

$$h = K^{\left(\frac{1}{1-n}\right)} \qquad \text{Eq. 2-59}$$

adding all the parameters identified before, h is calculated as Eq. 2-60 shows:

$$h = \left(13687 \cdot We_l^{0.1993} \cdot Re_l^{-0.1626} \cdot \left(\frac{T_w - T_{ref}}{\rho \cdot u \cdot (h_g - h_f)}\right)^{0.1993}\right)^{(1.2489)} \qquad \text{Eq. 2-60}$$

As an example, the physical properties of the refrigerant (R410A) in its phase change are detailed in Table 2-5. Moreover, Table 2-6 shows corresponding physical properties of saturated liquid and vapour refrigerant at 7.5 bars.

Table 2-5: List of physical properties of the refrigerant (R410A) used in the model.

Quality	Enthalpy [J/kg]	Density [kg/m^3]
0	197000	1178
0.1	219400	234.9
0.2	241700	130.5
0.3	264100	90.37
0.4	286500	69.12
0.5	308900	55.97
0.6	331300	47.03
0.7	353700	40.56
0.8	376000	35.65
0.9	398400	31.81
1	420800	28.72

Table 2-6: List of physical properties of the refrigerant (R410A) used in the model at 7.5 bars.

Physical properties	Symbol	Units	Value
Saturated temperature	T_{sat}	C	-2.04
Density liquid saturated	ρ_s	Kg/m^3	1178
Density vapour saturated	ρ_l	Kg/m^3	28.7
Conductivity liquid saturated	k_l	W/m·K	0.10460
Conductivity vapour saturated	k_v	W/m·K	0.01225
Enthalpy liquid saturated	λ_l	J/kg	197000
Enthalpy vapour saturated	λ_v	J/kg	420800
Specific heat liquid saturated	$C_{p,s}$	J/K·kg	1508
Specific heat vapour saturated	$C_{p,l}$	J/K·kg	1113

2.4.4 Water control volume

There is no water flow during a charging process, so $\dot{m}_{in} = \dot{m}_{out} = 0$. On the other hand, in a discharging process $\dot{m}_{in} = \dot{m}_{out}$.

$$\dot{Q}_{conv,P} - \dot{Q}_{conv,M} + \dot{Q}_{cond,N-1} - \dot{Q}_{cond,N+1} + (\dot{m}_{in} \cdot h_{in}) - (\dot{m}_{out} \cdot h_{out}) = \rho \cdot Cp \cdot \frac{(T_N^{t+1} - T_N^t)}{\Delta t} \cdot dV \quad \text{Eq. 2-61}$$

A typical correlation for forced convection in smooth tubes, turbulent flow is shown in Eq. 2-62

$$Nu = 0.023 \cdot Re^{0.8} \cdot Pr^n \quad \text{Eq. 2-62}$$

where Re is the Reynolds number and Pr the Prandt number, calculated using Eq. 2-63 and Eq. 2-64, respectively. The exponent n is 0.4 for heating of the fluid and 0.3 for cooling of the fluid.

$$Re = \frac{u \cdot L}{v} \quad \text{Eq. 2-63}$$

$$Pr = \frac{C_p \cdot \mu}{k} \quad \text{Eq. 2-64}$$

where u is the velocity of the fluid, L is the characteristic linear dimension, v is the kinematic viscosity of the fluid, C_p is the specific heat, μ is the dynamic viscosity, and k is the thermal conductivity.

If the channel through which the fluid flows is not of circular cross section, it is recommended that the heat-transfer correlations be based on the hydraulic diameter (D_h) defined by Eq. 2-65.

$$D_h = \frac{4 \cdot A}{P} \quad \text{Eq. 2-65}$$

where A is the cross-sectional area of the flow and P is the wetted perimeter.

It is also defined the heat-transfer for fully developed laminar flow ($Re<10^3$) in ducts with a variety of flow cross sections. In particular, for the geometry analysed here, Nusselt number for a constant axial wall temperature of 7.541.

The physical properties of the water are detailed in Table 2-7.

Table 2-7: List of physical properties of the refrigerant (R410A) used in the model.

Physical properties	Symbol	Units	Value
Conductivity (T=0.01 C)	k	W/m·K	0.55575
Conductivity (T=10 C)	k	W/m·K	0.57864
Density (T=0.01 C)	ρ	Kg/m^3	999.9
Density (T=10 C)	ρ	Kg/m^3	999.7
Specific heat (T=0.01 C)	C_p	J/K·kg	4219.9
Specific heat (T=10 C)	C_p	J/K·kg	4195.5
Kinematic viscosity (T=0.01 C)	ν	m^2/s	0.00000179180
Kinematic viscosity (T=10 C)	ν	m^2/s	0.00000130650

2.4.5 PCM control volume

PCM (lower: M) control volume

$$\dot{Q}_{conv,N} - \dot{Q}_{cond,M+1} + \dot{Q}_{\boldsymbol{cond},M-1} - \dot{Q}_{cond,M+1} = \rho \cdot Cp \cdot \frac{(T_M^{t+1} - T_M^t)}{\Delta t} \cdot dV \quad \text{Eq. 2-66}$$

PCM (middle: M+1) control volume

$$\dot{Q}_{cond,M} - \dot{Q}_{cond,M+n} + \dot{Q}_{cond,(M+1)-1} - \dot{Q}_{cond,(M+1)+1} = \rho \cdot Cp \cdot \frac{(T_{M+1}^{t+1} - T_{M+1}^t)}{\Delta t} \cdot dV \quad \text{Eq. 2-67}$$

PCM (upper: M+n) control volume

$$\dot{Q}_{cond,M+1} - \dot{Q}_{\boldsymbol{conv},P} + \dot{Q}_{cond,(M+n)-1} - \dot{Q}_{cond,(M+n)+1} = \rho \cdot Cp \cdot \frac{(T_{M+n}^{t+1} - T_{M+n}^t)}{\Delta t} \cdot dV \quad \text{Eq. 2-68}$$

RT4 from Rubitherm has been selected for the initial numerical experimentation in the Mediterranean concept. The physical properties of the PCM used in the model are detailed in Table 2-8 and the specific heat is shown in Figure 2-24.

Table 2-8: List of physical properties of the PCM (RT4-Rubitherm) used in the model.

Physical properties	Symbol	Units	Value
Density @ solid	ρ_s	Kg/m^3	880
Density @ liquid	ρ_l	Kg/m^3	770
Conductivity	k	W/m·K	0.2
Enthalpy	λ	J/kg	160000
Temperature of fusion	T_{PC}	C	0-4.5
Specific heat @ solid	$C_{p,s}$	J/K·kg	2000
Specific heat @ liquid	$C_{p,l}$	J/K·kg	3000

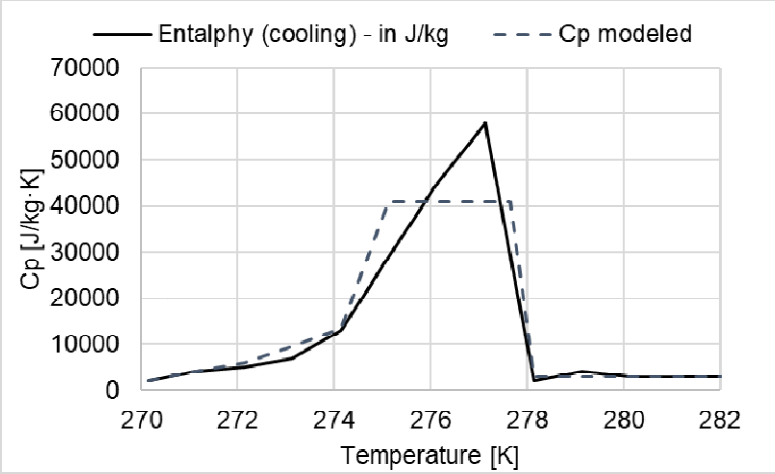

Figure 2-24: Specific heat in function of the temperature for RT4 and for the PCM modelled.

2.4.6 Phase transition models for technical-grade PCM

Phase transitions are modeled based on the general assumption, that the overall structure of the PCM can be approximated by two phases, a solid and a liquid phase. For technical grade PCM, as manufactured e.g. by Rubitherm GmbH [30], the phase change does not occur at an exact temperature, but rather within a specific temperature range. This means that it is assumed that the two phases coexist during solid/liquid phase transition and allows to approximate the overall structure of the PCM by one characteristic parameter $\xi \in [0,1]$,

$$\xi := \frac{m^l}{m^l + m^s} \qquad \text{Eq. 2-69}$$

denoting the (liquid mass) phase fraction, and m^s and m^l are the masses of solid and liquid phase, respectively. Most simple models for the phase transition (from solid with $\xi = 0$ to liquid with $\xi = 1$) assume that the phase fraction is a direct function of temperature: $\xi := \xi(T)$. In the following $\xi(T)$ is referred to as "transition function".

$$\xi(T) := \int_{-\infty}^{T} \phi(T)\, dT \quad \text{with} \quad \int_{-\infty}^{\infty} \phi(T)\, dT = 1 \qquad \text{Eq. 2-70}$$

In Eq. 2-70, $\phi(T)$ might be expressed by a (continuous) probability distribution function, or simply density function. Accordingly, $\xi(T)$ is then the corresponding cumulative density function. These functions are convenient as they can be parametrized by a relatively small number of location and shape parameters, and as they always preserve the integral value of one. E.g. Uzan et al. [31] models $\phi(T)$ as Gaussian density functions.

In this contribution, two density functions are taken from NIST/SEMATECH [32]. In contrast to the Gaussian PDF, these PDF have a closed (analytic) form of the respective cumulative density function and thus, are easier to implement in different software environments. Firstly, the Gumbel Minimum (Extreme Value Type I) density function NIST/SEMATECH [32]:

$$\phi^G(\tau;\mu,\beta) = \frac{1}{\beta}\exp\left(\frac{\tau-\mu}{\beta}\right)\exp\left(-\exp\left(\frac{\tau-\mu}{\beta}\right)\right) \qquad \text{Eq. 2-71}$$

where μ, β are location and shape parameters.

Secondly, because of the higher shape flexibility an adapted Weibull density function [32] is also considered (adaptation, mirrored around μ):

$$\phi^W(\tau;\gamma,\mu,\alpha) = \begin{cases} \frac{\gamma}{\alpha}\left(-\frac{\tau-\mu}{\alpha}\right)^{\gamma-1}\exp\left(\left(\frac{\tau-\mu}{\alpha}\right)^{\gamma}\right), & \tau < \mu \\ 0, & \tau \geq \mu \end{cases} \qquad \text{Eq. 2-72}$$

where μ, γ, α are location and shape parameters.

Eq. 2-69 shows two exemplary realizations of the Gumbel Minimum and adapted Weibull density functions and their corresponding cumulative density functions. The cumulative density functions are models for the "transition function" ξ(T) in Eq. 2-70.

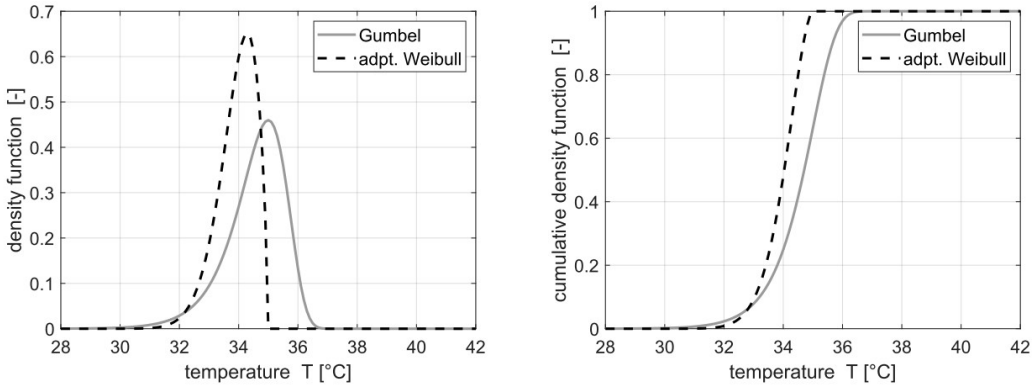

Figure 2-25: Gumbel Minimum (Eq. 2-71) and adapted Weibull (Eq. 2-72) density functions (left), and corresponding cumulative density functions (right).

2.4.7 PCM property models

Apparent specific heat capacity modeling

A generic two phase model for the apparent (or effective) specific heat capacity $\tilde{c}$ of the PCM is given by a linear superposition of terms for liquid (c_p^l) and solid (c_p^s) heat capacity as well as the latent heat (Δh) released or absorbed in the phase transition region [33]:

$$\tilde{c} := \underbrace{\xi c_p^l + (1-\xi)c_p^s}_{\text{sensible heat}} + \underbrace{\frac{\partial \xi}{\partial T}\Delta h}_{\text{latent heat}} \qquad \text{Eq. 2-73}$$

Note that in Eq. 2-73, ξ is a transition function and depends on temperature, i.e. $\xi = \xi(T)$, see Eq. 2-70. Possible models for ξ and its derivative $d\xi/dT$ have been proposed in section 2.4.5, where ξ is modeled by a cumulative density and $d\xi/dT$ is its corresponding density function.

Apparent density and thermal conductivity modeling

For the technical-grade PCM hereby considered, it has been assumed that solid and liquid phases coexist within the phase transition temperature range. It is therefore also assumed that within this temperature range, all PCM thermophysical properties can be modeled by a superposition of contributions from pure solid and pure liquid PCM properties. This superposition gives an apparent (or effective) PCM property. In the sensible heat model in Eq. 2-73, contributions from liquid and solid heat capacity are weighted by the liquid mass fraction $\xi(T)$. Accordingly, the transition function $\xi(T)$ are used to compute the weights and the following relation is used for modeling apparent density and thermal conductivity:

$$\tilde{\rho} := \xi\rho^l + (1-\xi)\rho^s \qquad \text{Eq. 2-74}$$

$$\tilde{\lambda} := \xi\lambda^l + (1-\xi)\lambda^s \qquad \text{Eq. 2-75}$$

2.4.8 Identification of phase transition and property models for PCM RT4

The phase transition models in section 2.4.6, i.e. models for $\xi := \xi(T)$, can be (indirectly) identified by fitting the apparent specific heat capacity model Eq. 2-73 to caloric measurement data of the PCM. The fitting is performed by numerical solution of a nonlinear regression problem.

Results are discussed for Rubitherm's PCM RT4, see Figure 2-26 for corresponding caloric measurement data provided by the PCM manufacturer.

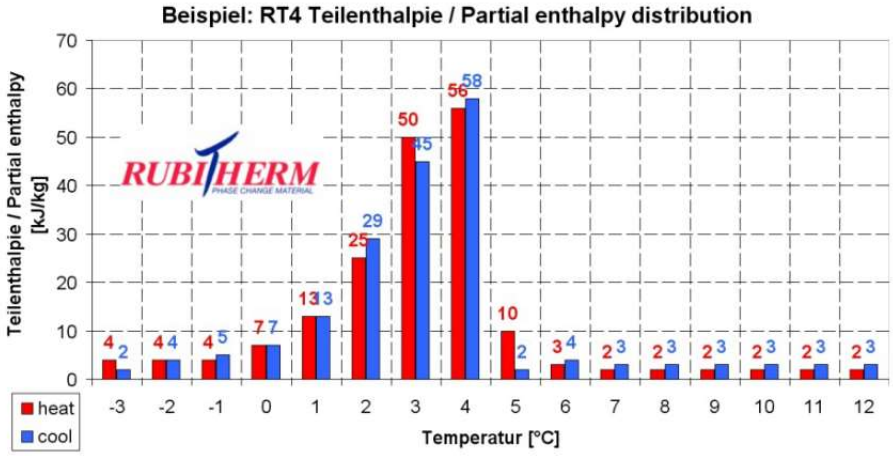

Figure 2-26: Caloric data for RT4 as provided by Rubitherm Technologies GmbH Techdata.

Two different results from fitting the apparent specific heat capacity model in Eq. 2-73 to the data in Figure 2-26 are presented.

- Fitting RT4 heating and cooling data simultaneously, see Figure 2-27, left:

  The corresponding phase transition model is shown in Figure 2-28, left. The identified regression parameters are: ϕ = Gumbel; μ = 276.7635; β = 0.8812; Δh = 1.3912e + 05; $c_p^s = c_p^l = 3.0374e + 03$.

  This is probably the preferred option if the focus is on both, good predictive model performance for charging and discharging storage operation.

- Fitting RT4 cooling data only, see Figure 2-27, right:

  The corresponding phase transition model is shown in Figure 2-28, right. The identified regression parameters are: ϕ = adptWeibull; μ = 278.1495; α = 2.1080; γ = 1.5087; Δh = 1.5563e + 05; $c_p^s = c_p^l = 2.9443e + 03$.

  This is probably the preferred option if the focus is on exact model predictions for discharging the storage/ cooling the PCM.

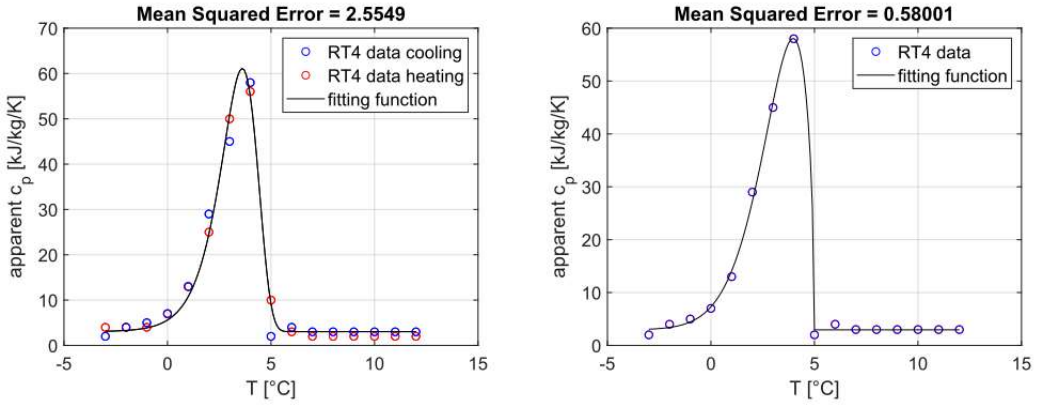

Figure 2-27: Apparent specific heat capacity model for Rubitherm RT4. Left: Experimental data for heating and cooling was fitted simultaneously using Gumbel density function (see Figure 2-28 (left) for corresponding identified phase transition model). Right: Experimental data for cooling was fitted using adapted Weibull density function (see Figure 2-28 (right) for corresponding identified phase transition model).

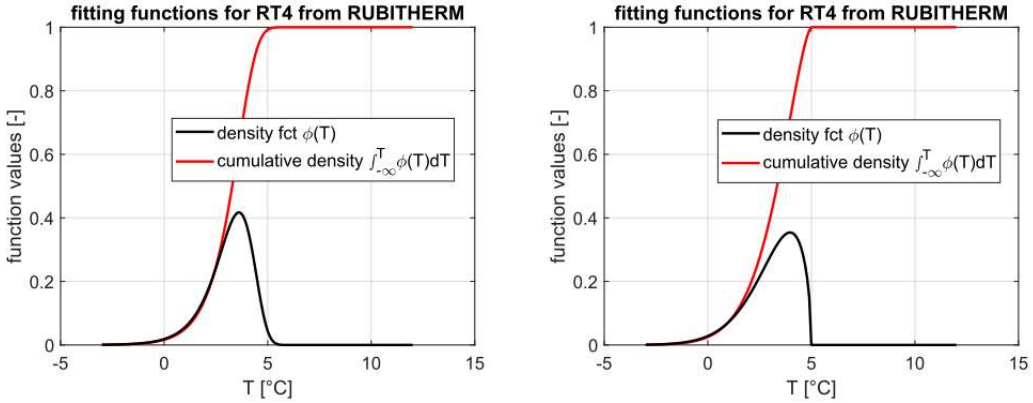

Figure 2-28: Different phase transition models ξ(T) (red line) obtained from fitting Rubitherm's PCM RT4 caloric data. Left: using Gumbel Minimum density (and cumulative density) function in Eq. 2-71. Right: using adapted Weibull density (and cumulative density) function in Eq. 2-72.

Note that, the fitting of cooling data only (Figure 2-27, right) leads to more asymmetric shape of the fitted apparent specific heat capacity model. Thus, it can be expected that using this model the discharging process is closer to the "ideal PCM behavior" than the charging process.

2.4.9 Derivation of apparent density and thermal conductivity models

Available density and thermal conductivity data for RT4 from Rubitherm is given in Table 2-9.

Table 2-9: Density and thermal conductivity data for RT4 as provided by Rubitherm Technologies GmbH Techdata

Density solid (at 15° C)	0.88 kg/l
Density liquid (at 15° C)	0.77 kg/l
Thermal conductivity	0.2 $Wm^{-1}K^{-1}$

In Table 2-9 it can be seen that data for pure solid and pure liquid density is available. Corresponding values, namely ρ^s= 0.88 kg/l and ρ^l= 0.77 kg/l, are used with Eq. 2-74. Results are shown for both phase transition models in figure 3.5:

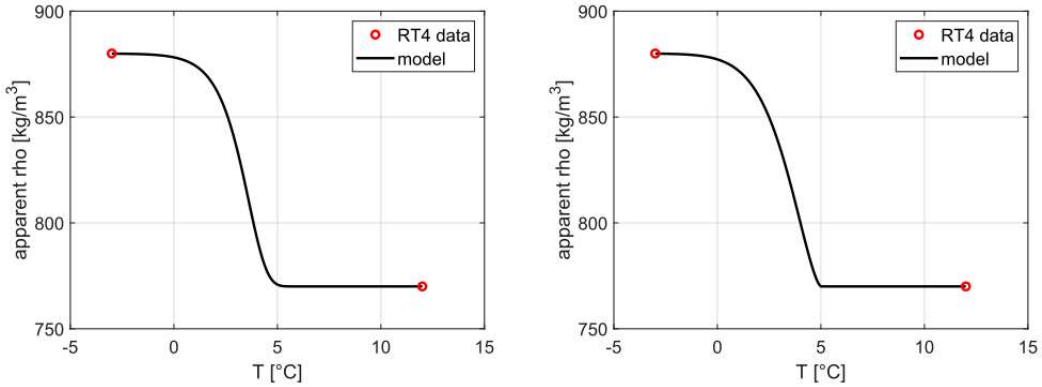

Figure 2-29: Apparent density $\tilde{\rho}$ model for Rubitherm RT4. Left: Using Gumbel density function (see Figure 2-28 (left) for corresponding phase transition model). Right: Using adapted Weibull density function (see Figure 2-28 (right) for corresponding phase transition model).

Moreover, because there is only one data point for thermal conductivity, thermal conductivity is assumed constant, and Eq. 2-75 is replaced by λ = 0.2 W/m/K.

2.4.10 Identification of phase transition and property models for PCM RT64HC

PCM RT64HC has been selected for the CON system. Caloric measurement data provided by the PCM manufacturer is given in Eq. 2-75.

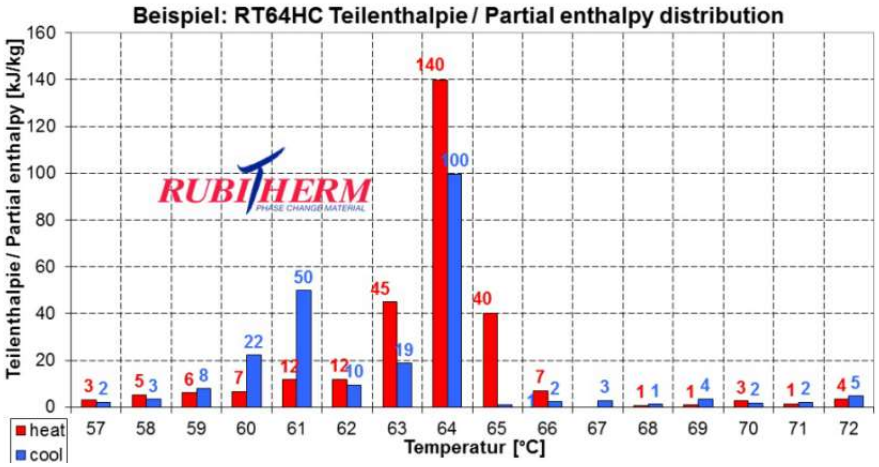

Figure 2-30: Caloric data for RT64HC as provided by Rubitherm Technologies GmbH Techdata.

Density and thermal conductivity data is given in figure 4.2.

Density solid at 20 °C	**0,88**	**[kg/l]**
Density liquid at 80 °C	**0,78**	**[kg/l]**
Heat conductivity (both phases)	**0,2**	**[W/(m·K)]**

Figure 2-31: Density and thermal conductivity data for RT64HC as provided by Rubitherm Technologies GmbH Techdata.

Using this data, the same steps are applied as in sections 2.4.8, 2.4.9, and models for $\tilde{c}$ and density $\tilde{\rho}$ are derived, the thermal conductivity is set to λ = 0.2.

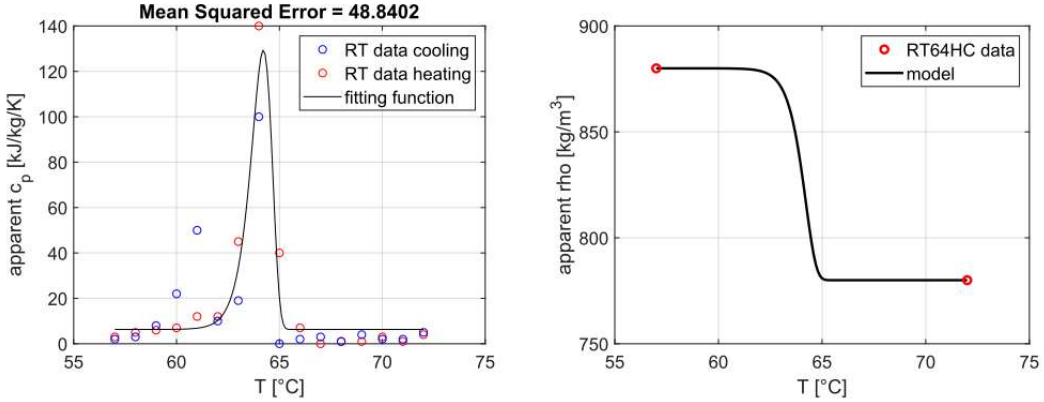

Figure 2-32: Results from the fitting experimental data for heating and cooling using Gumbel density function. Left: Apparent specific heat capacity $\tilde{c}$ model for Rubitherm RT64HC. Right: Apparent density $\tilde{\rho}$ model for Rubitherm RT64HC.

The identified regression parameters are: ϕ = Gumbel; μ = 337.3677; β = 0.5031; Δh =1.6834e+05; $c_p^s = c_p^l = 6.2964e+03$.

2.4.11 Determination of the state of charge of the RPW-HEX

The following definition originally proposed by Barz et al. [34] is used to define the state of charge (SoC) of the RPW-HEX.

Definition (State of charge of a latent thermal storage with solid/liquid PCM). *The term state of charge (SoC) and the symbol Ξ are used to indicate the extent to which a latent thermal storage is charged relative to storable latent heat. The SoC Ξ is calculated as the geometric mean of local (liquid mass) phase fraction fields ξ(x,y,z), where x, y, z represent spatial coordinates of the PCM contained in the latent thermal storage.*

The local phase fraction values are defined by the transition functions in 2.4.6. They can be directly derived from local temperatures. Accordingly, temperature fields T(x, y, z) in the PCM can be directly transformed into phase fraction fields ξ(x, y, z).

The RPW-HEX is a rectangular container. The internal design consists of a parallel arrangement of rectangular passages for water and refrigerant with rectangular layers of PCM in between. Fluid passages and PCM layers are arranged sequentially. Because of symmetry of the RPW-HEX design, the relatively abundance of passages and layers, and the thermal insulation of the storage container it is assumed that all parallel passages and PCM layers behave identically. Thus, storage internal temperature and phase fraction fields can be represented by one PCM layer only. Moreover, it is further assumed that the three-dimensional planar geometry can be reduced to a two dimensional geometry, with a coordinate pointing in the water or refrigerant flow direction (x on the domain $0 \le x \le L$), and one coordinate pointing into the PCM layer perpendicular to the first coordinate (y on the domain $0 \le y \le d$). For this two-dimensional planar geometry of the PCM, the state of charge Ξ is calculated as geometric mean as:

$$\Xi = \frac{\int_0^L \int_0^d \xi(x,y)\, dy\, dx}{L \cdot d} \qquad \text{Eq. 2-76}$$

The integration of Eq. 2-76 needs to be carried out numerically.

For the Continental system the RPW-HEX is used as hot storage, while for the Mediterranean system it is used as cold storage. Accordingly, different SoC are defined to account for the fact that the hot storage is fully charged if all PCM is in the liquid state, while the cold storage is fully charged when the PCM is in solid state:

$$\Xi^{\text{hot}} := \Xi$$
$$\Xi^{\text{cold}} := 1 - \Xi \qquad \text{Eq. 2-77}$$

2.4.12 Interface to the hybrid subsystem model - Dymola implementation of the RPW-HEX model

The numerical RPW-HEX model developed by UDL has been implemented in Modelica/Dymola simulation software in order to facilitate subsystem simulations for the MED and CON system, and to develop and evaluate its design and basic control settings under different operating scenarios. A minimal test example (no connection to other subsystem components) for the Mediterranean system is shown in Figure 2-33.

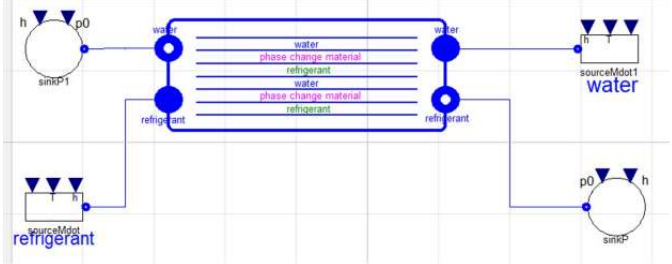

Figure 2-33: Dymola RPW-HEX model object of the Mediterranean system. This minimal test example uses

fixed water and refrigerant inlet conditions.

The user interface for the definition of main RPW-HEX parameters is shown in Figure 2-34.

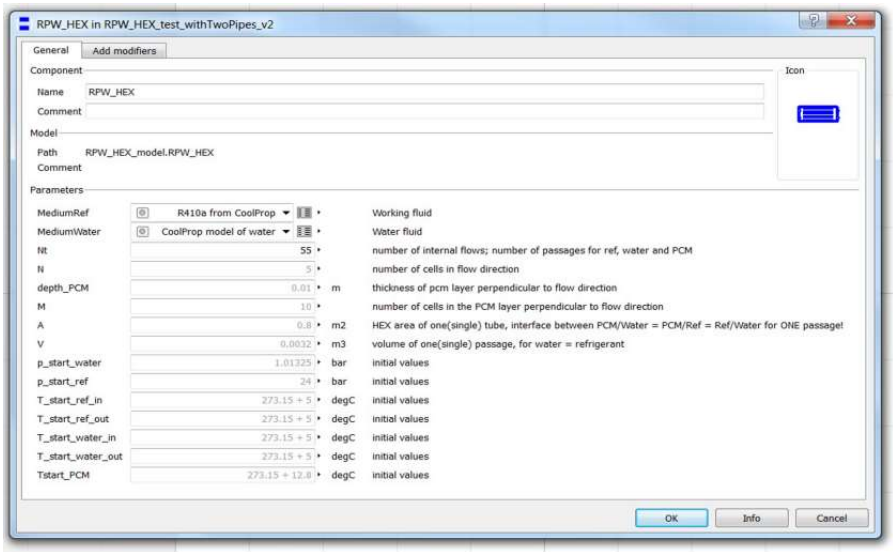

Figure 2-34: Parameter list of the Dymola RPW HEX model object of the Mediterranean system: working fluids, geometry data, numerical grid data, and initial values for simulation.

The model adopts the assumptions and basic balance equations of the UDL 3-fluid heat exchanger model, see section 2.4.2. The implementation is based on the state-of-the-art ThermoCycle library model components (see [3]). These model components are used to represent the water and refrigerant flow through the RPW-HEX internal parallel passages. Corresponding components are modifications of ThermoCycles so called “Flow1D” and “Cell1D” fluid flow components, see Figure 2-35. Modifications concern the addition of a second heat port to account for: heat transfer between water (or refrigerant) passage and PCM, and heat transfer between water and refrigerant passage. This approach is in line with the model developed by UDL (the three-fluid heat exchanger model in sections 2.4.1-2.4.7). The use of ThermoCycle standard fluid flow components, enables the user to select between different (available) options for state-of-the-art numerical discretization schemes and options for well-established heat transfer correlations, e.g. the first order upwind discretization scheme and Shahs heat transfer correlations (see section 2.4.3).

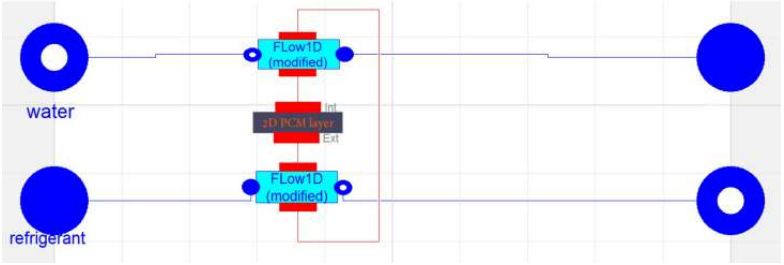

Figure 2-35: Graphical representation of model classes used to define the Dymola RPW-HEX model of the Mediterranean system. Heat ports and connectors between the balance envelops of the water passage, refrigerant passage and the PCM layer are shown in red.

The PCM layer is modeled using a ThermoCycle adapted heat flow component, namely a wall element. This component can be directly connected to the fluid flow elements using

ThermoCycle thermal ports. According to the three-fluid HEX model developed by UDL in sections 2.4.1-2.4.7, a two-dimensional PCM model is implemented and apparent (effective) PCM properties are used. The user can select between different phase transition models, as proposed in sections 2.4.7 to 2.4.10, and the SoC is calculated as defined in section 2.4.11.

2.5 Electrical storage model (ITAE)

2.5.1 Introduction

Batteries can be described by means of electrochemical or analytical models [35], the latter one having the significant advantage to describe the behavior of the battery by using a reduced number of equations. The model can be then calibrated by means of experimental testing to derive the operating parameter for each technology and specific cell. Such an approach holds another advantage over electrochemical models, i.e. the possibility to easily adapt the model to make good estimations of the SoC for battery packs [36].

2.5.2 Methodology

One of the most used analytical models based on an equivalent electric circuit is Sheperd models, that describes the electrochemical behavior of a battery in terms of voltage and current by excluding thermal and quantum phenomena [37], [38]. One drawback in the use of this model is that it does not take into account capacity reduction with increasing of discharging current [39]. Indeed, during a discharge at high current rate, the speed of the electrochemical process does not allow to discharge the total capacity stored in a battery[40]. In order to take such a phenomenon into account the model was improved by introducing the Peukert equation that quantifies the capacity reduction according to output current from the battery [41]. The Thevenin equivalent circuit used as reference is shown in Figure 2-36. The main elements in the electric circuit are: two generators, to take into account the hysteresis between charge and discharge, a series resistance R_0, to model the internal resistance of the battery, and a parallel between a resistance R_1 and a capacity C. The resistance R_1 is the polarization resistance and it has the function to model the diffusion process of the lithium ion. The capacity C describes the transient response of the battery during a charge or a discharge [42].

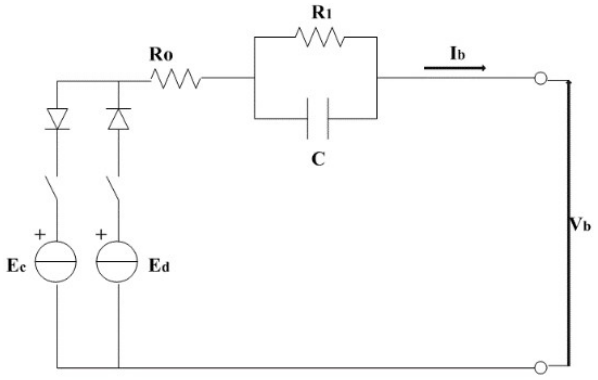

Figure 2-36: Equivalent circuit for the battery model.

2.5.3 Model description

The model developed is based on the following assumptions:

- constant battery parameters in different thermal conditions;
- variable internal resistance with the SoC level;
- experimental relation between OCV (Open Circuit Voltage) and state of charge SoC level;
- no self-discharge.

The reference equations of the model are the following:

$$V = E_0 - J\frac{C_{max}}{C_{max} - C(t)}i + H\,exp[-P \cdot C(t)] - R_0 i \quad \text{Eq. 2-78}$$

$$V = E - R_0 i \quad \text{Eq. 2-79}$$

where: V is the cell voltage [V], E_o the Open Circuit Voltage(OCV) [V], J the polarization factor [Ah^{-1}], C_{max} the maximum capacity of the battery [Ah], C(t) the charged/discharged capacity at time t, i the cell current [A], H the exponential voltage component [V], P the exponential capacity component [Ah^{-1}], R_0 the internal resistance [Ω].

With reference to Figure 2-36, the voltage of the cell V is equal to E_c during charge and E_d during discharge.

The SOC is estimated as:

$$SOC = \int \frac{i}{C_{max}} dt \quad \text{Eq. 2-80}$$

2.5.4 Model validation

The model was validated using the experimental data on a testing setup present at ITAE and described in [43]. The validation on a charging/discharging profile is shown in for a LiFePO4 cell for different types of tests. It is possible to notice that the model follows the dynamic evolution and SOC for all the cases, thus being able to reproduce the behavior of the component, see Figure 2-37.

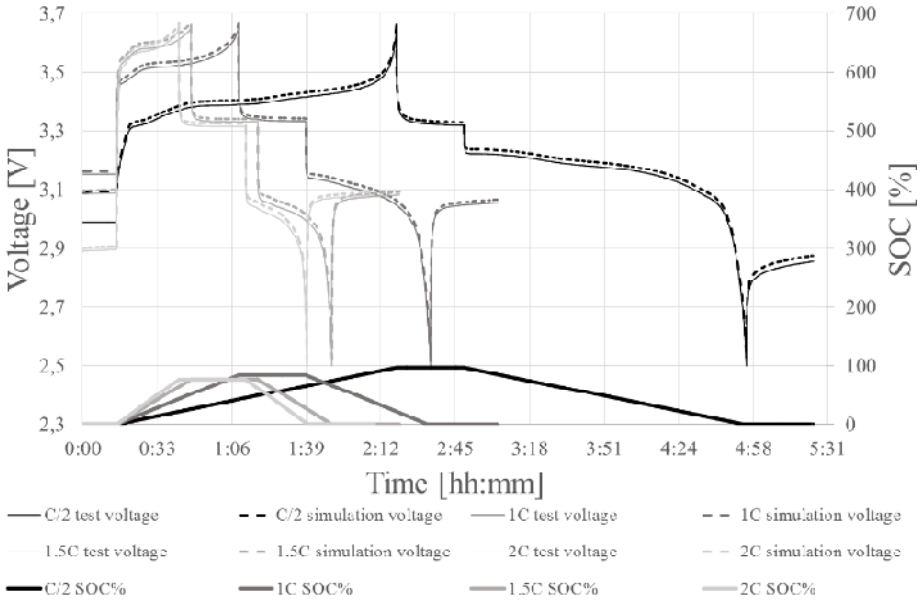

Figure 2-37: Validation of the battery model.

2.6 Auxiliary models

2.6.1 Charge controller (ITAE)

A charge controller was modelled in order to regulate the energy flow of the electrical storage according to operating conditions and external conditions. In particular, the inputs to the charge controller are:

- voltage, current and SoC of the battery;
- current and voltage of the load;
- current and voltage of the source (e.g. PV panels or electric grid).

Moreover, the following parameters are introduced:

- minimum SoC allowed to start discharge;
- minimum voltage allowed to start discharge
- maximum current allowed during charge/discharge;
- maximum voltage allowed during charge;
- minimum voltage and current from the source to start charge.

From the comparison of the input values and the parameters, one of three operating modes is activated:

- charge of the battery;
- discharge of the battery;
- self-consumption, i.e. the power generated from the source is directly passed to the load.

Moreover, manual operation of the controller is possible, in order to take into account possible predictive control logics (e.g. based on weather forecasts or price of electricity).

Dymola diagram of the charge controller is shown in Figure 2-38.

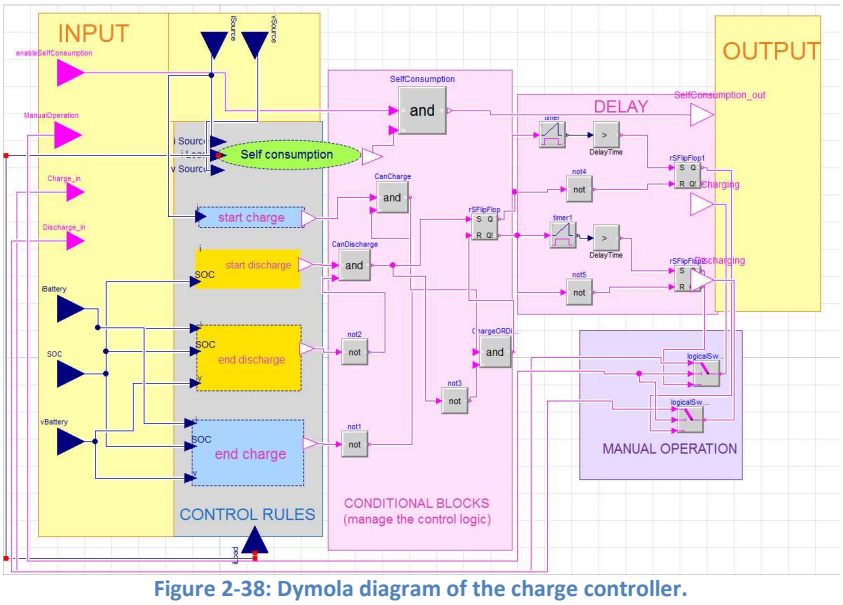

Figure 2-38: Dymola diagram of the charge controller.

2.6.1.1 *Typical example*

An example of the results of the simulation for a cell with nominal voltage of 3 V and periodically charged/discharge is shown in Figure 2-39.

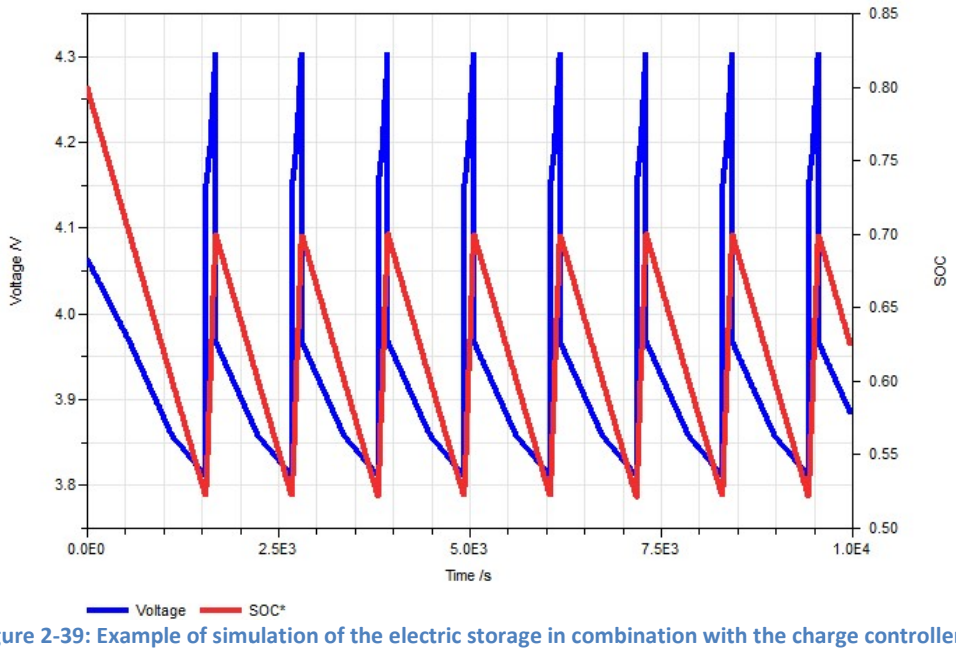

Figure 2-39: Example of simulation of the electric storage in combination with the charge controller.

2.6.2 Simple Building Model (AIT)

Although building simulations are carried out in detail in WP4, T3.1 suggests two simplified methods to test the hybrid sub-systems with simplified building models in T3.1 before detailed simulations of the buildings become available. The two methods are described in the following

with the aid of the Continental demo site in Talence. Please note, that these methods are also applicable for the Mediterranean demo site. Which one of the two described methods is needed depends on the timescale of the problem.

Timescale of a year for techno-economic analysis, economic design decisions of single sub-system components and performance map generation

A set of reduced operating conditions for one typical year to test the models in a valid range, create performance maps and to calculate seasonal efficiencies is needed. Based on this set, e.g. the seasonal efficiencies can be calculated by simulating each operating condition of the set in the steady state and summing up the energy demand over a year on an hourly basis (Bin-method). At a timescale of a year, this quasi-static method is preferred to dynamic simulations if such a high level of details as in the models of T3.1 is used. Figure 2-40 shows a set of reduced operating conditions calculated from preliminary results of simulations of the thermal energy demand of the Continental demo building. The hourly based data (8760 operating conditions, see also the cyan-coloured dots in Figure 2-41) were reduced first to 414 operating conditions by collecting the hourly based data in data bins of the size 1 K for the outlet air temperature (t_{ODA}) and 500 W for the heating/cooling demand ($\dot{Q}$). Secondly, solely the operating conditions responsible for 95% of all operating hours (operating hours >4 h/year) were considered to reduce the number of operating conditions further to 233 conditions. For the reduced set of operating conditions, simulations can be carried out to calculate the steady-state conditions of individual sub-systems at these points. This information can be used for the techno-economic analysis, the performance maps for WP4 and for design decisions in WP3.

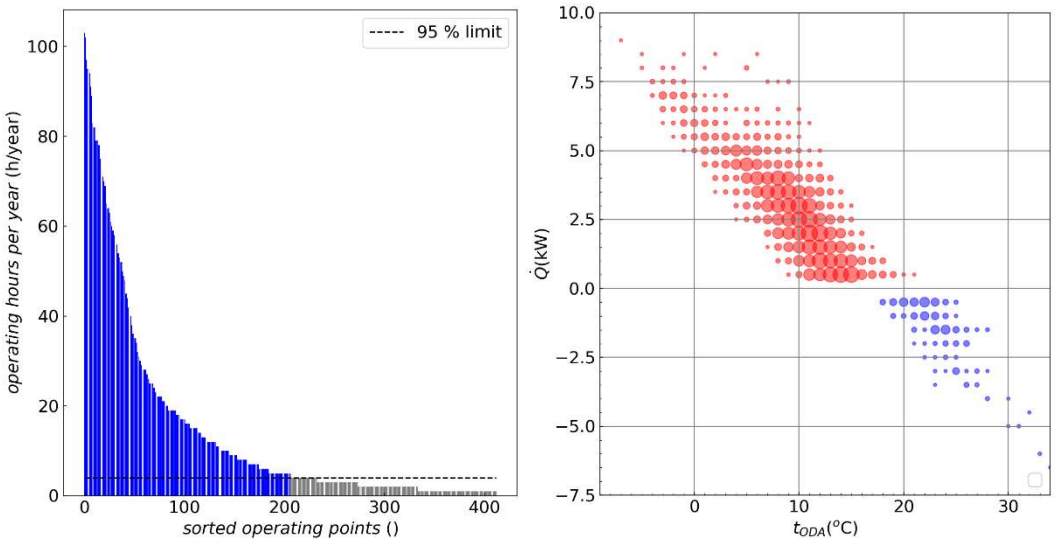

Figure 2-40: Occurrence (frequency) of operating conditions (left) and reduced set of operating conditions (right) for the Continental demo building in Talence. For each data point depicted in the reduced set, the operating conditions in the range of ± 0.5 K and ± 250 W were collected from the hourly based data. The area of the circles in the right figure is proportional to the occurrence of the operating point during the year.

Timescale of (sub-)seconds for low-level control strategies and technical design decisions of single sub-system components

A model that represents the dynamic behaviour on a small timescale is also needed in T3.1. With the aid of this model, control strategies on the lower level can be found, clever interconnections can be identified, and single components of the hybrid sub system can be

designed. In other words, correlations between the temperature of the heating/cooling distribution system, the building temperature and the ambient temperature are needed. Furthermore, the Domestic Hot Water (DHW) consumption and the solar yield from PV needs to be addressed.

With the aid of such a model, the dynamic behaviour of the system can be tested at certain operating points.

Contrary to the detailed models of the buildings which will be developed in WP4, we

- use linear heat transfer correlation and
- neglect solar radiation, radiation losses and wind speeds

to calculate the thermal energy demand of the building in our simplified model. The following equations are used to describe the heating ($\dot{Q}_h$) and cooling ($\dot{Q}_c$) demand of the building:

$$\dot{Q}_h = UA_h\ ((t_b - \Delta t) - t_{ODA}) \qquad \text{Eq. 2-81}$$

$$\dot{Q}_c = UA_c\ (t_b + \Delta t) \qquad \text{Eq. 2-82}$$

where UA represents a heat transfer coefficient for heating and cooling, respectively, t_b is the temperature of the building and Δt addresses a temperature bandwidth in which either heating or cooling is needed. Figure 2-41 shows the least square fit of Eq. 2-81 and Eq. 2-82 to the data points of preliminary calculated heating and cooling demands of the Continental demo building. Please note that, the two equations were connected by a tanh-transfer function in the final model and in Figure 2-41 to guarantee numerical robustness:

$$\dot{Q}_{amb} = \dot{Q}_h \frac{1 + \tanh\left(\varepsilon\left(t_b - t_{ODA} - \frac{\Delta t}{2}\right)\right)}{2} + \dot{Q}_c \frac{1 - \tanh\left(\varepsilon\left(t_b - t_{ODA} - \frac{\Delta t}{2}\right)\right)}{2} \qquad \text{Eq. 2-83}$$

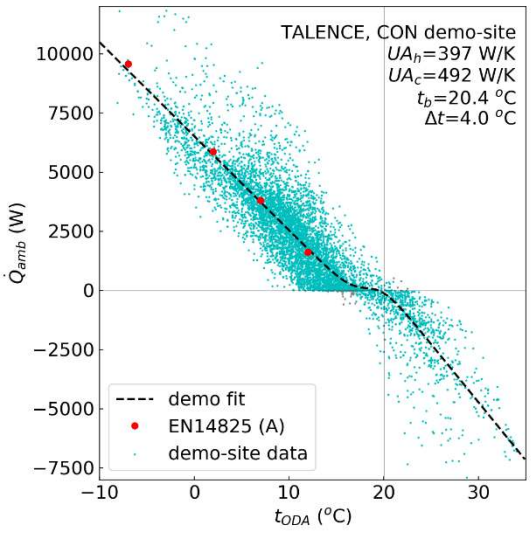

Figure 2-41: Least square fit of the preliminary calculated heating and cooling demand provided by the demo site in France (Talence) according to (1) and (2).

Since the inlet temperatures to the heating/cooling distribution system were not available yet, we use temperature dependencies from the EN14825 standard [44]. In the EN14825, part load

conditions for heat pumps in three different climate zones (warm, average, cold) and for four different heating applications (low temperature, intermediate temperature, medium temperature and hot temperature) are listed. We choose the average climate and the intermediate temperature application for the Continental demo-site. By comparing the red circles with the fit curve and the demo-site data in Figure 2-41, we see a good agreement between the average climate condition and the demo-site. Figure 2-42 shows the correlation between the return temperature of the fluid in the heating/cooling distribution system and the transferred heat from the fluid into the building, if a temperature difference of 5 K between inlet and return temperature is maintained by an external variable speed pump.

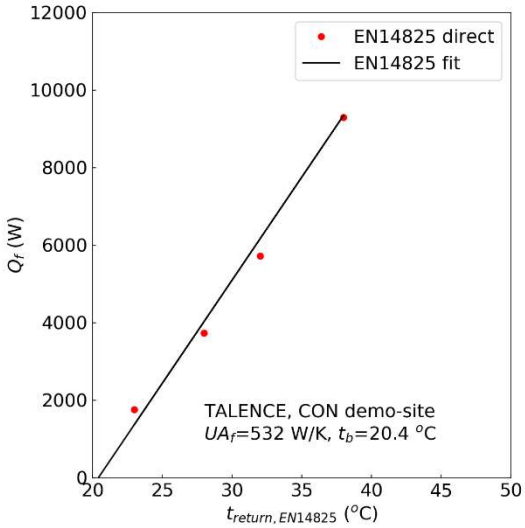

Figure 2-42: Transferred heat from the heating distribution system into the building according to the EN14825 for average climate and intermediate heating applications.

Again, the transferred heat from the fluid to the building ($\dot{Q}_f$) is fitted with a linear equation:

$$\dot{Q}_f = UA_f\ (t_f - t_b) \qquad \text{Eq. 2-84}$$

where t_f represents the return temperature (=outlet temperature of building).

Both heat transfer equations are connected with each other via an energy balance considering the thermal mass of the building $M_b c_b$:

$$M_b c_b\ \dot{t}_b = \dot{Q}_f - \dot{Q}_{amb} \qquad \text{Eq. 2-85}$$

Inserting the values of the fitting parameters $UA_h, UA_c, UA_f, \Delta t$ in in Eq. 2-81 to Eq. 2.85, one finds for all four test points of the EN14825 (red circles) a building temperature t_b of about 20.4°C in the steady-state.

In the small timescale case, also the DHW consumption is of importance. The ThermoCycle-library offers different models to describe a DHW storage (e.g. the ThermoclineStorage model). Hence, there is no need for developing a model for the DHW storages, one can use the external models directly with the HYBUILD models. Artificial DHW consumption profiles for heat pump system can be taken from sources like the EN16147 standard.

3 The hybrid sub-system models

3.1 The Mediterranean hybrid sub-system (ITAE)

3.1.1 Overview

The Mediterranean hybrid sub-system comprises four main components: the sorption module, the compression heat pump, the RPW-HEX module, and the electrical storage. The main interfaces of each component with the others in the sub-system were described more in detail in the previous sections. Figure 3-1 shows the Dymola diagram of the complete subsystem, including the sources and sinks that simulate the other components in the overall system and the electric parameters from the PV panels. The integration of the heat pump with the RPW-HEX is shown in detail in Figure 3-2. What is clear is that the approach followed proved to be effective, since it was easily possible to connect all the components and realize a complete model of the subsystem.

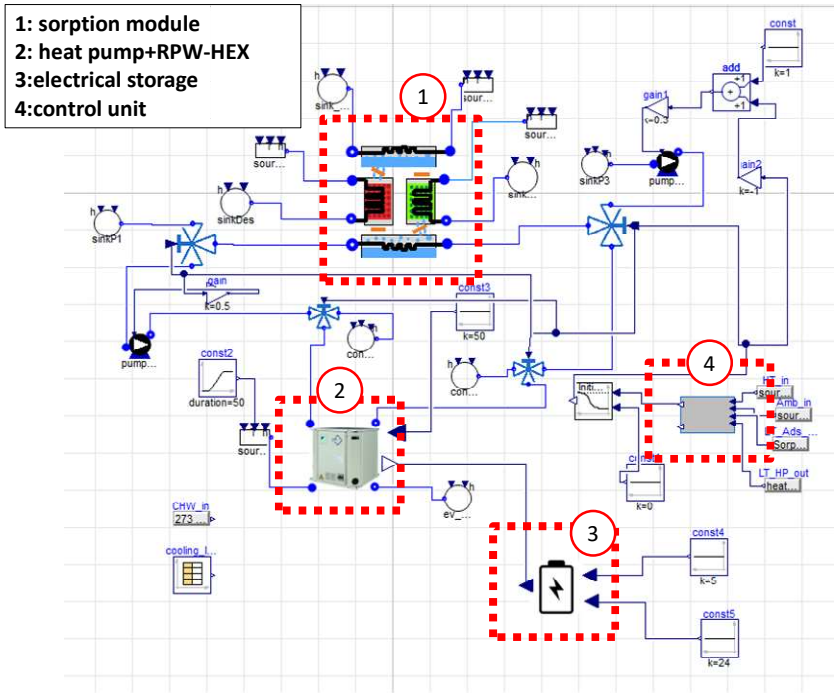

Figure 3-1: Dymola diagram of the Mediterranean subsystem.

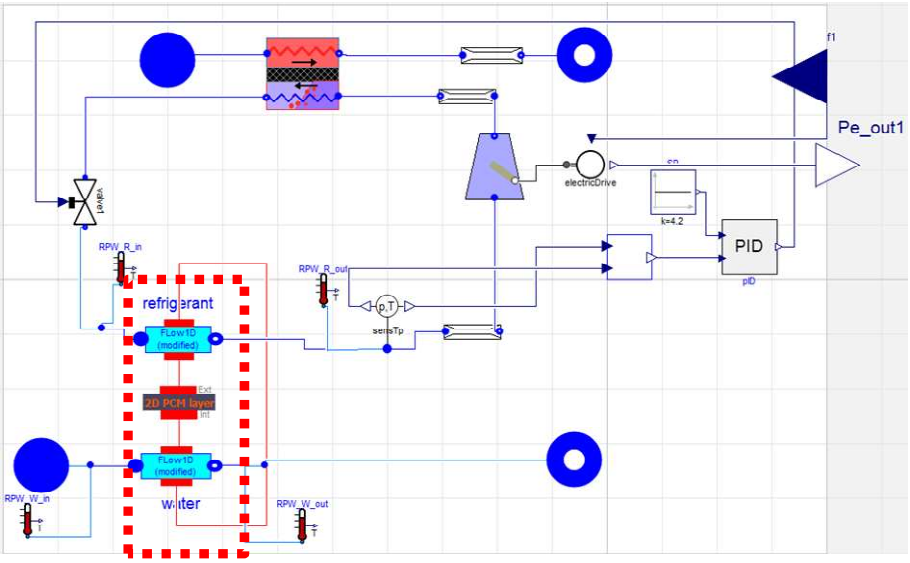

Figure 3-2: Detail of the integration of the heat pump with the RPW-HEX.

3.1.2 Basic control

In order to run the model and carry out some preliminary simulations, basic control logics were applied. Indeed, the development of the model of a control unit, (component (4) in Figure 3-1), allows for an easier integration of the detailed control logics that will be defined within T4.2. Presently, the following main conditions were applied in order to run the adsorption module:

- the temperature of the heat source is higher than a user-defined value (in the present case, 75°C);
- the temperature in the chilled water circuit (evaporator secondary circuit) of the adsorption unit is lower than T_{amb}-5°C, the condition under which direct connection of the compression unit with the external sinks becomes more favourable.

Moreover, a variable speed driver was predisposed, to match the supply frequency to the electric drive of the heat pump according to the actual cooling load.

3.1.3 Reference conditions for testing of the integrated model

In order to test the model of the sub-system, data available for the demo site in Aglantzia were used. In particular, based on ASHRAE design conditions for Cyprus, the selected reference day is in August and has a peak ambient temperature of 35°C. The cooling load and ambient temperature for the selected days that were used as boundary conditions for the model, are shown in Figure 3-3.

For simplicity's sake a constant heat source temperature of 90°C was considered, taking into account that the heat coming from the solar Fresnel collectors in the installation will be collected in a sensible storage.

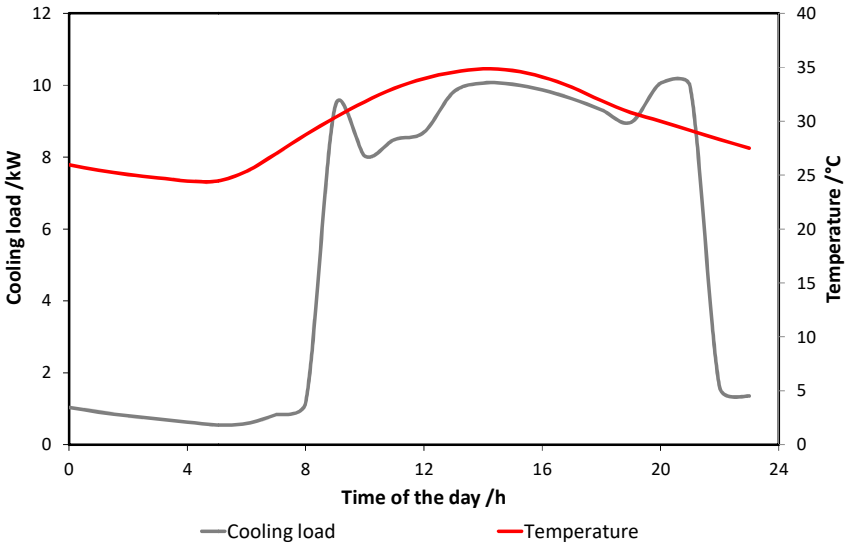

Figure 3-3: Cooling load and temperature for a reference day in August for the demo site in Aglantzia.

3.1.4 Typical example

Using the abovementioned boundaries, the model of the entire sub-system was run. In particular, simulations from 9:00 to 15:00 were performed, and some cycles are shown in Figure 3-4 and Figure 3-5. In particular, Figure 3-4 shows the temperatures in the circuits of the adsorption module and the heat pump. The temperatures in the condenser circuit of the heat pump correspond with the temperatures of the circuit of the adsorption heat pump since, for the tested boundaries, they are always directly connected. It is possible to notice that the cyclic operation of the adsorption chiller induces periodic rising in the temperature of the condenser of the heat pump, but the average inlet to the condenser of the heat pump is below 20°C, thus reducing of more than 10°C the temperature lift of the unit.

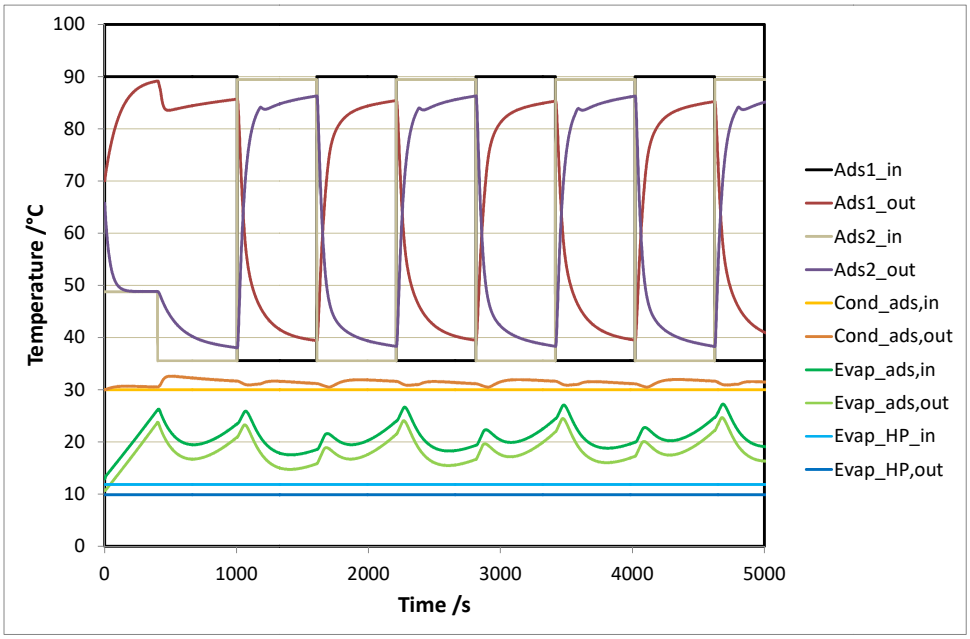

Figure 3-4: Temperatures in the circuits of the sorption module and heat pump for the reference conditions.

Figure 3-5 shows the powers in the different components of the adsorption module and the heat pump, calculated from the thermodynamic states of the fluids in each component. It is possible to notice that the power in the condenser of the heat pump corresponds to the average power from the evaporator of the adsorption module. Moreover, at each phase change there is a peak in the power absorbed/released from the adsorbers, due to the sensible heat and sorption heat of the material.

Finally, another simulation was run with constant boundary temperatures: 90°C heat source, 30°C ambient temperature and return chilled water temperature of the heat pump variable from 15°C to 10°C. The aim was to identify the behaviour of the RPW-HEX. Results are reported in Figure 3-6, where 6 temperatures are reported: the suffix “ext” and “int” refers to the layer of the PCM (internal is the layer closer to the HTF, whereas external is the layer closer to the refrigerant) and the suffixes 1 to 10 refer to the node in the direction of the HTF. It is however worth noticing that the results for this component need to be strongly validated after experimental campaign at UDL.

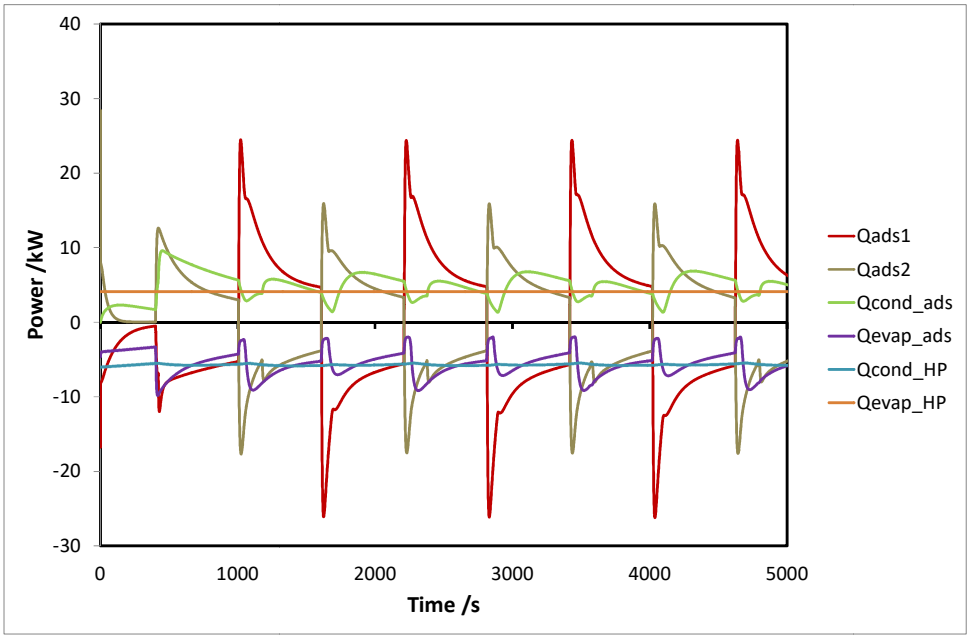

Figure 3-5: Thermal powers in the components of the sorption module and the heat pump for the reference conditions.

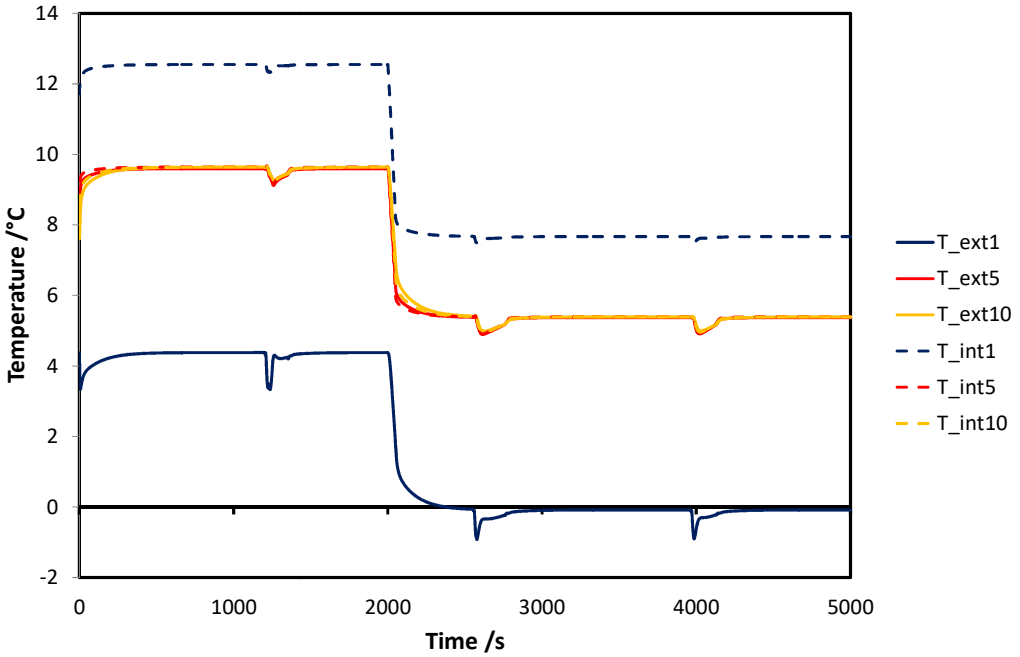

Figure 3-6: Temperatures in different layers and nodes of the PCM in the RPW-HEX.

3.1.5 Outcomes

The model of the sub-system was primarily meant to obtain information on the performance of the sub-system itself and optimise component sizing and basic controls. To this aim, it is already predisposed to test different control logics. Indeed, inside the heat pump model (not shown in Figure 3-1) the possibility to switch between the evaporator and the RPW-HEX module is implemented. At the same time, the possibility to connect the chiller to the sorption storage or directly to the dry cooler was foreseen. Finally, also the integration of the electric storage with the chiller is considered, since the power required from the chiller is passed as an input to the model of the electric storage, in order to define whether it can be supplied by the battery or by the external sources.

Once the model of each component will be experimentally validated, the model can be used for the final sizing of the components and the definition of the optimal control logic and operating modes based on external conditions (e.g. temperatures and load).

3.2 The Continental hybrid sub-system (AIT)

3.2.1 Overview

As already shown in Figure 2, the Continental hybrid sub-system consists of mainly three main components: the compression heat pump system including the outdoor air source HEX (see section 2.3), the integrated RPW-HEX (see section 2.4) and the battery (see section 2.4.1). For the sake of simplicity, we show in Figure 3-7 solely the thermal sub-system in the Dymola/Modelica software environment. The battery can be integrated similar as already shown with the Mediterranean concept. The outdoor unit (A) and the RPW-HEX (C) are directly integrated in a compression heat pump cycle together with the conventional components compressor (B), condenser (D) and expansion valve (E). The PID Controllers (F) and (G) control the rotational speed and the opening degree of the expansion valve, respectively. The heating load of the building is represented with the simple building model (H, see also section 2.6.2),

and the decentralized DHW storage is represented with a thermocline storage from the Thermocycle library (I). Two three-way valves (J, see also see section 2.2.2.5) change the hydraulic flow of the process water from heating to DHW-generation operation.

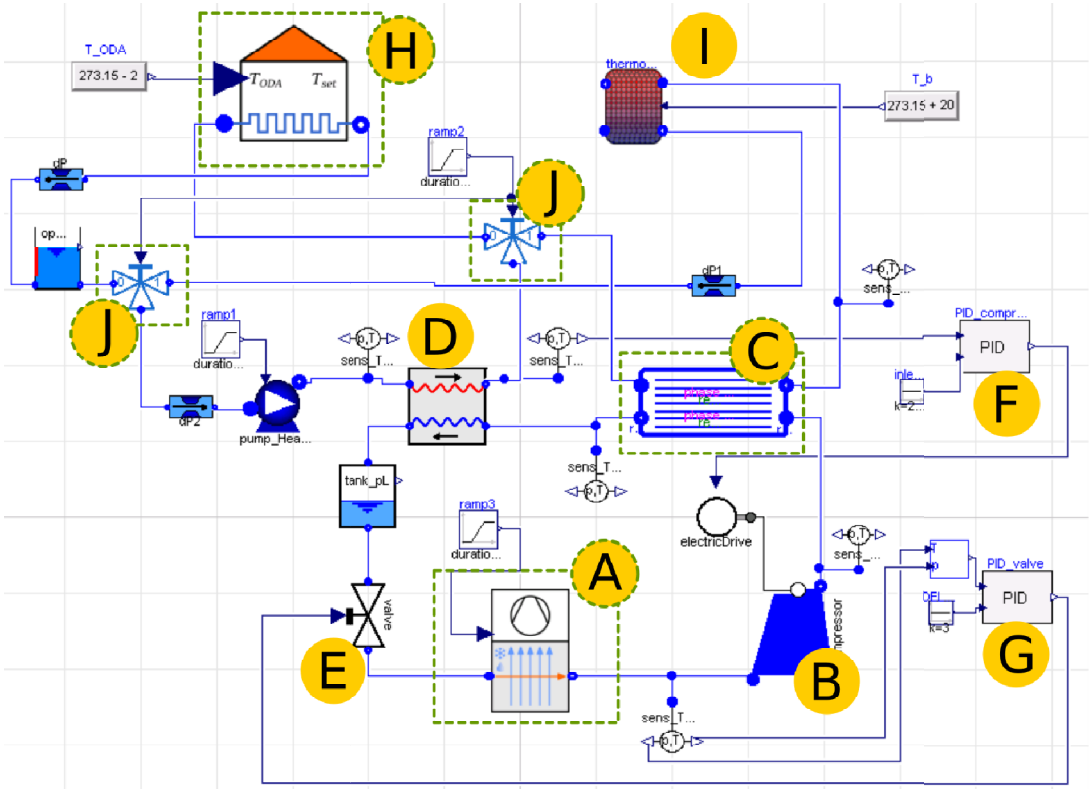

Figure 3-7: Schema of Continental thermal sub-system implemented in the Dymola environment. Components surrounded by green dashed rectangles indicate that they were developed in Task 3.1. (A) Continental outdoor unit (evaporator), (B) compressor, (C) RPW-HEX, (D) condenser, (E) expansion valve, (F) PID controller compressor, (G) PID controller expansion valve, (H) simplified building model, (I) decentralized DHW storage in the apartment, (J) three-way valves.

3.2.2 Basic control

The basic control strategy was implemented with two PID Controllers to control the superheating of the refrigerant leaving the evaporator and to control the outlet temperature of the process water at the condenser. The manipulated variable is the opening degree of the expansion valve and the rotational speed of the compressor, respectively. The parameter of the two PID controllers were first estimated with the aid of the Ziegler-Nichols tuning method without the RPW-HEX. After the integration of the RPW-HEX, the parameters of the PID controller for the rotational speed of the compressor had to be adapted to ensure a stable control whereas the values to control the expansion valve were kept from the Ziegler-Nichols method. Compared to the heat pump without RPW-HEX, the proportional gain of the PID controller for the compressor had to be reduced by a factor of about 200, whereas the integration time constant had to be raised by a factor of about 150 to guarantee a stable control with the latent storage.

Additionally, two three-way valves (J) were used to switch between DHW and heating/cooling operation. A ramp-source from the MSL was used to switch the three-way valves between 0 and 1 over a timespan of two seconds to ensure a smooth transition. A second ramp-source

was used to slow down the process water pump during DHW generation to 300 l/h and a third ramp-source slowed down the fan of the outdoor unit during DHW generation by a factor of two.

Please note that the Continental scheme in Figure 3-7 shows only one possible option for the hydraulic connections in the Continental system. The final scheme will be an outcome of WP3.

3.2.3 Reference conditions for testing of the integrated model

Preliminary data from the Continental demo-site in Talence are used to test the Continental sub-system. In the example in Figure 3-7 the building model for the small timescale (see section 2.6.2) was used to provide the correct response from the building.

3.2.4 Typical example

In the following we discuss the Continental sub-system at a typical operation conditions in winter. The outdoor temperature was set to 2°C in this scenario. The building itself is already heated to its steady-state temperature of 20.4 °C at t=0 s. The DHW storage needs to be charged and had an initial temperature of 15 °C at the bottom of the water tank and 35°C at the top (see Figure 3-9a). The RPW-HEX is filled with a RT64HC PCM material, which has a switching temperature at around 64 °C (see Figure 2-30 and Figure 2-32). At t=0 s the RPW-HEX has a uniform temperature of 62 °C, hence nearly no latent energy is stored at the beginning of the simulation (SoC = 1.2 %).

After starting the heat pump at t=0 s in heating mode (no mass flow to the decentralized DHW storages), we switch the system after 4000 s to DHW generation mode. For a fair comparison we will observe solely the behavior of the system after stabilization of the heat pump between SoCs of 5 % or in other words between t=426 s and t=4714 s (see Figure 3-8). Hence, the building heating time will last for around 1 hour before the heat pump switches for 12 minutes into DHW generation mode. During heating operation, the RPW-HEX will be charged up to a maximum of 35 % before we switch the hydraulic valves to DHW generation and slow down the process water and the RPW-HEX will be discharged down to 5 % (see Figure 3-8). Contrary to conventional systems, the condensing pressure/temperature controlled via the temperature of the process water outlet and the compressor rotational speed should stay nearly the same during heating and DHW generation operation. The extra thermal energy to heat up the process water to DHW-temperatures (>60°C) will solely be extracted from the RPW-HEX in DHW generation mode. In Figure 3-9b (green, dashed line) one can see that the implemented PID-controller does not manage to limit the outlet condenser temperature $\vartheta_{wa,con}^{(out)}$ perfectly during DHW generation, what is a difficult task as the compressor speed (and therefore the power consumption) decreases (see Figure 3-10a) and the inlet temperature to the secondary side of the condenser $\vartheta_{wa,con}^{(in)}$ (blue solid line in Figure 3-9b) varies constantly. One can see clearly, that the stored energy in the RPW-HEX is sufficient to provide process water with a charging temperature of about 63°C (red dotted line in Figure 3-9b) for about 12 minutes which heats the top layer or the decentralized storage to about 50°C.

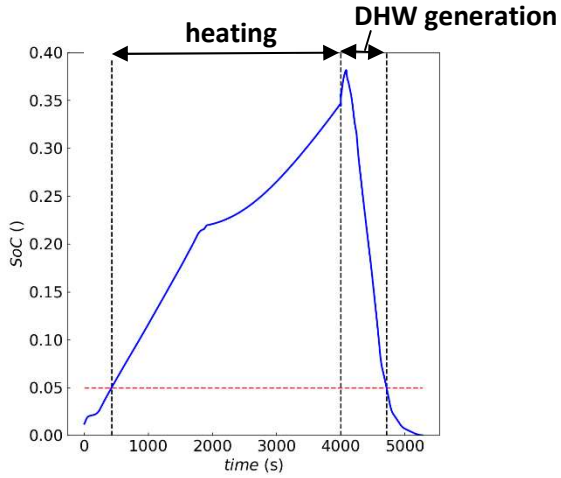

Figure 3-8: State of Charge (SoC) of the RPW-HEX.

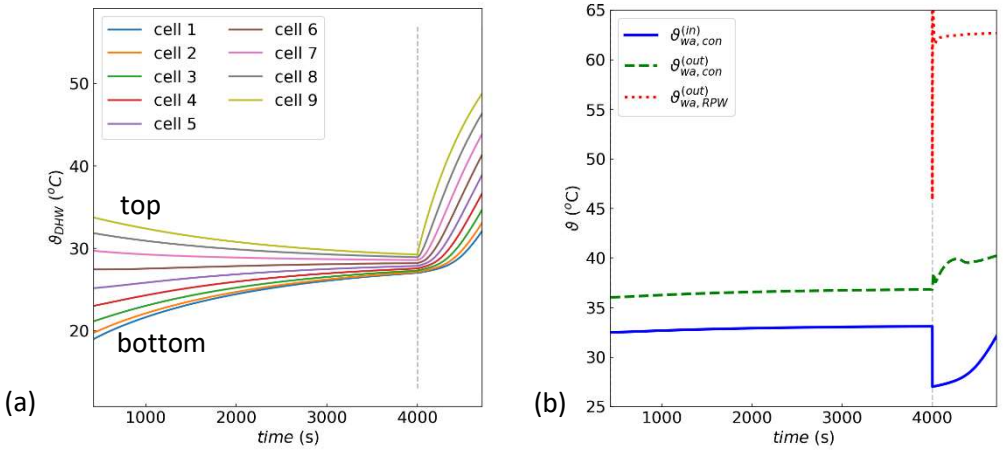

Figure 3-9: Vertical temperature distribution in the decentralized DHW-storage from the top (cell9) to the bottom (cell1) (a) and temperatures on the process water side of the condenser and the RPW-HEXFigure (b)

During heating mode a thermal energy of Q_{heati} = 6.67 kWh is transferred to the building, whereas the thermal energy of Q_{DHW} = 2.3 kWh is transferred to the DHW storage in DHW-generation mode (see Figure 3-10b). Note, that 2.3 kWh is approximately the thermal energy needed for DHW for one person per day. Out of this 2.3 kWh, 1.55 kWh were provided by the hot gas and the PCM during DHW generation and the rest (0.75 kWh) was provided via the condenser of the heat pump. The overall COP for the compressor over one cycle of heating and DHW generation can be calculated with:

$$COP_{comp} = \frac{Q_{heating} + Q_{DHW}}{E_{comp}} \quad \text{Eq. 3-1}$$

and we find a COP_{comp} of 4 for heating **and** DHW-generation in the Continental concept. This is the same COP_{comp} as conventional systems have for heating operation only, whereas typical DHW generation COPs are considerably lower than 3.

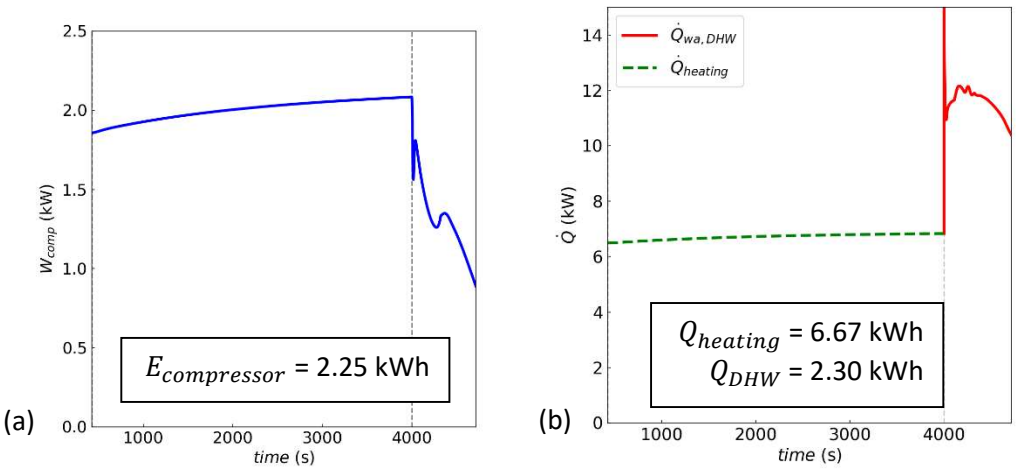

Figure 3-10: Power consumption of the compressor (a) and heat transfer to the process water during heating DHW-generation (b)

With the presented example, we have demonstrated, that the HYBUILD concept is able to provide thermal energy for heating and DHW with the same highly efficient COP as conventional systems reach for heating, only. This is possible because of the storage of the thermal energy extracted from the hot gas in the RPW-HEX during heating operation and later utilization of the stored energy for DHW generation.

3.2.5 Outcomes

The model of the Continental sub-system was already used for first performance analysis and to find first reasonable parameters for the heat pump controller. Different connections on the secondary side were already simulated and the one presented in Figure 3-7 represent the most promising at this point of time. After validation of the single component- and the sub-system-models the validated models will be used further for sizing, techno-economic analysis, controller development and testing of different interconnections.

4 Conclusions

Dynamic simulation models for the core components and modules of the HYBUILD hybrid sub-systems were successfully developed in Task 3.1. The developed models for each component proved to be flexible and reliable. Typical examples showed how each of the components work in the Dymola/Modelica environment. In a further step, the developed components were connected with each other and to open source components from the Modelica Standard Library or the ThermoCycle Library to simulate the Mediterranean and the Continental sub-systems as a whole. Preliminary simulation results from WP4 and data delivered by the demo-sites were used as constraints to test the simulation models of the entire sub-systems, whereby different ways of considering these constraints were shown in the examples. The results of the entire sub-system simulations confirmed the ability of the model to simulate detailed operation of each component of the sub-system and the ability to integrate the developed models into existing and freely available libraries.

As a preliminary attempt to tune the models, they were calibrated with existing data from datasheets or previous experiments in other projects. E.g. the Mediterranean heat pump and the adsorber models were calibrated against Daikin's and literature data respectively. The complete validation of the model will be performed out of the experimental characterization in Task 3.2, which will be carried out in the months to come in the labs of AIT, ITAE, NTUA and UDL. The validated models will then be used to:

- optimize the component sizing;
- optimize and test the control of the sub-systems;
- test different hydraulic interconnections;
- carry out a techno-economic analysis of the sub-systems.

5 References

[1] U. Bau, F. Lanzerath, M. Gräber, S. Graf, H. Schreiber, N. Thielen, and A. Bardow, "Adsorption energy systems library - Modeling adsorption based chillers, heat pumps, thermal storages and desiccant systems," in *Proceedings of the 10th International Modelica Conference*, 2014.

[2] F. Lanzerath, U. Bau, J. Seiler, A. Bardow, and E. Bardow, "Optimal design of adsorption chillers based on a validated dynamic object-oriented model," *Science and Technology for the Built Environment*, vol. 21, pp. 248–257, 2015.

[3] S. Quoilin, A. Desideri, J. Wronski, I. Bell, and V. Lemort, "ThermoCycle : A Modelica library for the simulation of thermodynamic systems," in *Proceedings of the 10th International Modelica Conference*, 2014.

[4] I. H. Bell, J. Wronski, S. Quoilin, and V. Lemort, "Pure and Pseudo-pure Fluid Thermophysical Property Evaluation and the Open-Source Thermophysical Property Library CoolProp," *Industrial & Engineering Chemistry Research*, vol. 53, no. 6, pp. 2498–2508, Feb. 2014.

[5] M. Schicktanz and T. Núñez, "Modelling of an adsorption chiller for dynamic system simulation," *International Journal of Refrigeration*, vol. 32, no. 4, pp. 588–595, Jun. 2009.

[6] A. Frazzica and A. Freni, "Adsorbent working pairs for solar thermal energy storage in buildings," *Renewable Energy*, vol. 110, pp. 87–94, Sep. 2017.

[7] I. I. El-Sharkawy, "On the linear driving force approximation for adsorption cooling applications," *International Journal of Refrigeration*, vol. 34, no. 3, pp. 667–673, May 2011.

[8] F. Lanzerath, J. Seiler, M. Erdogan, H. Schreiber, M. Steinhilber, and A. Bardow, "The impact of filling level resolved: Capillary-assisted evaporation of water for adsorption heat pumps," 2016.

[9] A. Sapienza, S. Santamaria, A. Frazzica, A. Freni, and Y. I. Aristov, "Dynamic study of adsorbers by a new gravimetric version of the Large Temperature Jump method," *Applied Energy*, vol. 113, pp. 1244–1251, Jan. 2014.

[10] A. Freni, G. Maggio, F. Cipitì, and Y. I. Aristov, "Simulation of water sorption dynamics in adsorption chillers: One, two and four layers of loose silica grains," *Applied Thermal Engineering*, vol. 44, pp. 69–77, 2012.

[11] A. Sapienza, A. Velte, I. Girnik, A. Frazzica, G. Füldner, L. Schnabel, and Y. Aristov, "Water - Silica Siogel" working pair for adsorption chillers: Adsorption equilibrium and dynamics," *Renewable Energy*, vol. 110, pp. 40–46, Sep. 2017.

[12] S. Bendapudi, J. E. Braun, and E. A. Groll, "A comparison of moving-boundary and finite-volume formulations for transients in centrifugal chillers Comparaison entre les formulations aux limites mobiles et ´ gimes transitoires des aux volumes finis pour les re refroidisseurs centrifuges," *International Journal of Refrigeration*, vol. 31, no. 8, pp. 1437–1452, 2008.

[13] M. Willatzen and N. B. O. L. Pettit, "A general dynamic simulation model for evaporators and condensers in refrigeration . Part I : moving-boundary formulation of two-phase flows with heat exchange ´ ne ´ ral dynamique pour e ´ vaporateurs et Mode condenseurs frigorifiques . Partic I : Formul," *International Journal of Refrigeration*, vol. 21, no. 5, pp. 398–403, 1998.

[14] J. G.-M. F. Vera-Garcıa J.M. Corberan-Salvador J.R. Garcia-Cascalesa, "Assessment of boiling and condensation heat transfer correlations in the modelling of plate heat exchangers," *International Journal of Refrigeration*, vol. 30, pp. 1029–1041, 2007.

[15] B. P. Rasmussen and B. Shenoy, "Dynamic modeling for vapor compression systems — Part II : Simulation tutorial Review Article Dynamic modeling for vapor compression systems — Part II : Simulation tutorial," *HVAC&R Reasearch*, vol. 9669, no. October, 2017.

[16] P. Byrne, J. Miriel, and Y. Lénat, "Modelling and simulation of a heat pump for simultaneous heating and cooling," *Building Simulation*, vol. 5, no. 3, pp. 219–232, 2012.

[17] S. Quoilin, A. Desideri, J. Wronski, I. Bell, and V. Lemort68, "ThermoCycle: A Modelica library for the simulation of thermodynamic systems," in *Proc. 10th Int. Model. Conf., Lund,Sweden*, 2014.

[18] "TIL Suite – Simulates thermal systems." 2018.

[19] C. Reichl, "Project description SilentAirHP, Available: https://www.ait.ac.at/en/research-fields/sustainable-thermal-energy-systems/projects/silentairhp/." 2015.

[20] K. Lee, W. Kim, and T. Lee, "A one-dimensional model for frost formation on a cold flat surface," *INTERNATIONAL JOURNAL OF HEAT AND MASS TRANSFER*, vol. 40, no. 18, pp. 4359–4365, 1997.

[21] C. J. L. Hermes, R. O. Piucco, J. R. B. Jr., and C. Melo, "A study of frost growth and densification on flat surfaces," *Experimental Thermal and Fluid Science*, vol. 33, no. 2, pp. 371–379, 2009.

[22] K. Prölss and G. Schmitz, "Modeling of Frost Growth on Heat Exchanger Surfaces," in *Proceedings of the 5th Modelica Conference pp. 509-516*, 2006.

[23] H. Qiao, V. Aute, and R. Radermacher, "Modeling of transient characteristics of an air source heat pump with vapor injection during reverse-cycle defrosting," *International Journal of Refrigeration*, vol. 88, pp. 24–34, 2018.

[24] H. Qiao, V. Aute, and R. Radermacher, "Dynamic modeling and characteristic analysis of a two-stage vapor injection heat pump system under frosting conditions," *International Journal of Refrigeration*, vol. 84, pp. 181–197, 2017.

[25] K. S. and U. Groß, "Luftseitiger Wärmeübergang und Druckverlust in Lamellenrohr-Wärmeübertragern," *KI Luft- und Kältetechnik*, vol. 36, no. 1, pp. 13–18, 2000.

[26] M. M. Shahs, "Evaluation of General Correlations for Heat Transfer During Boiling of Saturated Liquids in Tubes and Annuli," *HVAC&R Research*, vol. 12, no. 4, pp. 1047–1063, 2006.

[27] M. M. Shah, "Chart correlation for saturated boiling heat transfer: equations and further study," *ASHRAE transactions*, vol. 88, 1982.

[28] M. M. Shah, "A new correlation for heat transfer during boiling flow through pipes," *Ashrae Trans*, vol. 82, no. 2, pp. 66–86, 1976.

[29] R. Yun, J. H. Heo, Y. C. Kim, and J. T. Chung, "Convective boiling heat transfer characteristics of R410A in microchannels," 2004.

[30] Rubitherm GmbH, Aug-2018.

[31] A. Y. Uzan, Y. Kozak, Y. Korin, I. Harary, H. Mehling, and G. Ziskind, "A novel multi-dimensional model for solidification process with supercooling," *International Journal of Heat and Mass Transfer*, vol. 106, pp. 91–102, 2017.

[32] NIST/SEMATECH, "e-Handbook of Statistical Methods." 2015.

[33] U. Gaur and B. Wunderlich, "Heat capacity and other thermodynamic properties of linear macromolecules. II. Polyethylene," *Journal of Physical and Chemical Reference Data*, vol. 10, no. 1, p. 119, 1981.

[34] T. Barz, D. Seliger, K. Marx, A. Sommer, S. F. Walter, H. G. Bock, and S. Körkel, "State and state of charge estimation for a latent heat storage," *Control Engineering Practice*, vol. 72, pp. 151–166, 2018.

[35] N. Bizon, N. Mahdavi Tabatabaei, F. Blaabjerg, and E. Kurt, *Energy harvesting and energy efficiency : technology, methods, and applications*. p. 661.

[36] O. Tremblay and L.-A. Dessaint, "Experimental Validation of a Battery Dynamic Model for EV Applications," *World Electric Vehicle Journal*, vol. 3, no. 2, pp. 289–298, Jun. 2009.

[37] H. Zhang and M.-Y. Chow, "Comprehensive dynamic battery modeling for PHEV applications," in *IEEE PES General Meeting*, 2010, pp. 1–6.

[38] C. M. Shepherd, "Design of Primary and Secondary Cells," *Journal of The Electrochemical Society*, vol. 112, no. 7, p. 657, Jul. 1965.

[39] J.-H. Kim, S.-J. Lee, E.-S. Kim, S.-K. Kim, C.-H. Kim, and L. Prikler, "Modeling of Battery for EV using EMTP/ATPDraw," *Journal of Electrical Engineering and Technology*, vol. 9, no. 1, pp. 98–105, Jan. 2014.

[40] O. Veneri, F. Migliardini, C. Capasso, and P. Corbo, "Dynamic behaviour of Li batteries in hydrogen fuel cell power trains," *Journal of Power Sources*, vol. 196, no. 21, pp. 9081–9086, Nov. 2011.

[41] E. Leksono, I. N. Haq, M. Iqbal, F. X. N. Soelami, and I. G. N. Merthayasa, "State of charge (SoC) estimation on LiFePO4 battery module using Coulomb counting methods with modified Peukert," in *2013 Joint International Conference on Rural Information & Communication Technology and Electric-Vehicle Technology (rICT & ICeV-T)*, 2013, pp. 1–4.

[42] F. Sun, R. Xiong, H. He, W. Li, and J. E. E. Aussems, "Model-based dynamic multi-parameter method for peak power estimation of lithium–ion batteries," *Applied Energy*, vol. 96, pp. 378–386, Aug. 2012.

[43] A. Arista, M. Ferraro, F. Sergi, and V. Antonucci, "Dynamic Model of High-Performance Li-Ion Cells (LIFEP04, LI-POLYMERS and LIFP6 NBC) in Different Load Conditions," in *6th IC-EpsMso International Conference on Experiments/Process/System Modeling/Simulation/Optimization*, 2015.

[44] *Air conditioners, liquid chilling packages and heat pumps, with electrically driven compressors, for space heating and cooling — Testing and rating at part load conditions and calculation of seasonal performance*. European standard EN 14825, 2016.